FINNISH METEOROLOGICAL INSTITUTE
CONTRIBUTIONS

No. 66

THEORETICAL MODELING OF IONOSPHERIC ELECTRODYNAMICS INCLUDING INDUCTION EFFECTS

Heikki Vanhamäki

Department of Physical Sciences
Faculty of Science
University of Helsinki
Helsinki, Finland

ACADEMIC DISSERTATION in theoretical physics
To be presented, with the permission of the Faculty of Science of the University of Helsinki, for public critisism in Auditorium D101 at Physicum in Kumpula Campus (Gustaf Hällströmin katu 2a) on November 2nd, 2007, at 12 o'clock noon.

Finnish Meteorological Institute
Helsinki, 2007

ISBN 978-951-697-632-0 (paperback)
ISBN 978-952-10-4243-0 (PDF)
ISSN 0782-6117

Yliopistopaino
Helsinki, 2007

FINNISH METEOROLOGICAL INSTITUTE

Published by Finnish Meteorological Institute
(Erik Palménin aukio 1) , P.O. Box 503
FIN-00101 Helsinki, Finland

Series title, number and report code of publication
Contributions 66, FMI-CONT-66

Date October 2007

Authors

Heikki Vanhamäki

Name of project

Commissioned by

Title

Theoretical modeling of ionospheric electrodynamics including induction effects

Abstract

This thesis deals with theoretical modeling of the electrodynamics of auroral ionospheres. In the five research articles forming the main part of the thesis we have concentrated on two main themes: Development of new data-analysis techniques and study of inductive phenomena in the ionospheric electrodynamics. The introductory part of the thesis provides a background for these new results and places them in the wider context of ionospheric research.

In this thesis we have developed a new tool (called 1D SECS) for analysing ground based magnetic measurements from a 1-dimensional magnetometer chain (usually aligned in the North-South direction) and a new method for obtaining ionospheric electric field from combined ground based magnetic measurements and estimated ionospheric electric conductance. Both these methods are based on earlier work, but contain important new features: 1D SECS respects the spherical geometry of large scale ionospheric electrojet systems and due to an innovative way of implementing boundary conditions the new method for obtaining electric fields can be applied also at local scale studies. These new calculation methods have been tested using both simulated and real data. The tests indicate that the new methods are more reliable than the previous techniques.

Inductive phenomena are intimately related to temporal changes in electric currents. As the large scale ionospheric current systems change relatively slowly, in time scales of several minutes or hours, inductive effects are usually assumed to be negligible. However, during the past ten years, it has been realised that induction can play an important part in some ionospheric phenomena. In this thesis we have studied the role of inductive electric fields and currents in ionospheric electrodynamics. We have formulated the induction problem so that only ionospheric electric parameters are used in the calculations. This is in contrast to previous studies, which require knowledge of the magnetospheric-ionosphere coupling. We have applied our technique to several realistic models of typical auroral phenomena. The results indicate that inductive electric fields and currents are locally important during the most dynamical phenomena (like the westward travelling surge, WTS). In these situations induction may locally contribute up to 20-30% of the total ionospheric electric field and currents. Inductive phenomena do also change the field-aligned currents flowing between the ionosphere and magnetosphere, thus modifying the coupling between the two regions.

Publishing unit
Space Research Unit

Classification (UDK)
52

Keywords
Ionosphere, Electromagnetism

ISSN and series title
0782-6117 Finnish Meteorological Institute Contributions

ISBN
978-951-697-632-0 (paperback), 978-952-10-4243-0 (pdf)

Language
English

Sold by
Finnish Meteorological Institute / Library
P.O.Box 503, FIN-00101 Helsinki
Finland

Pages 170

Price

Note

ILMATIETEEN LAITOS

Julkaisun sarja, numero ja raporttikoodi
Contributions 66, FMI-CONT-66

Julkaisija Ilmatieteen laitos, (Erik Palménin aukio 1)
PL 503, 00101 Helsinki

Julkaisuaika Lokakuu 2007

Tekijä(t)

Heikki Vanhamäki

Projektin nimi

Toimeksiantaja

Nimeke

Ionosfäärin sähködynamiikan ja induktioilmiöiden teoreettisesta mallintamisesta

Tiivistelmä

Tässä väitöskirjassa käsitellään revontulialueiden ionosfäärin sähködynamiikkaa. Väitöskirjan ydinosa koostuu viidestä referoidusta artikkelista, joissa keskitytään kahteen pääteemaan: Kehitetään uusia menetelmiä mittausdatan käsittelyyn ja mallinnetaan ionosfäärin sisäistä sähkömagneettista induktiota. Väitöskirjan johdanto-osa antaa taustatietoa Maan lähiavaruudesta ja ionosfääritutkimuksesta, sekä asettaa artikkeleissa esitetyt uudet tulokset osaksi laajempaan kokonaisuutta.

Väitöskirjassa esitellään uusi työkalu (nimeltään 1D SECS) maanpinnalle, yleensä poihjoinen-etelä suuntaisesti sijoitettujen magnetometriketjujen havaintojen analysointiin. Lisäksi kehitetään toinen uusi menetelmä ionosfäärin sähkökenttien laskemiseen käyttäen lähtötietoina maanpinnalla mitattua magneettikenttää ja arviota ionosfäärin sähkönjohtavuudesta. Molemmat uudet menetelmät perustuvat osittain aikaisempiin tutkimuksiin, mutta sisältävät merkittäviä parannuksia: 1D SECS menetelmä huomioi ionosfäärin suuren skaalan sähkösuihkuvirtausten pallomaisen geometrian kun taas sähkökentän laskentaan tarkoitettua menetelmää voidaan käyttää luotettavasti myös paikallisissa tarkasteluissa, sillä se käsittelee alueen reunalla tarvittavat reunaehdot uudella tavalla. Esitettyjä menetelmiä testataan sekä erilaisia malleja että mittausdataa käyttäen. Testit osoittavat uusien menetelmät antavan aikaisempaa luotettavampia tuloksia.

Induktiiviset ilmiöt liittyvät läheisesti sähkövirtojen ajallisiin muutoksiin. Ionosfäärin suuren skaalan virtajärjestelmät muuttuvat melko hitaasti, minuuttien tai tuntien aikaskaaloissa, joten ionosfäärissä induktioilmiöiden on uskottu olevan merkityksettömiä. Kuitenkin viimeisten runsaan kymmenen vuoden aikana on huomattu induktiolla voivan olla suurta merkityssä eräissä ionosfäärin ilmiöissä. Väitöskirjassa tutkitaan induktiivisten sähkökenttien ja virtojen roolia ionosfäärin sähködynamiikassa. Induktio-ongelma muotoillaan siten että laskennassa tarvitaan pelkästään ionosfäärin sisäisiä sähköisiä parametreja. Tämä eroaa aikaisemmista lähestymistavoista, joissa ongelman ratkaisemiseksi tarvitaan tietoa ionosfäärin ja magnetosfäärin välisestä kytkennästä. Uutta laskentatekniikka sovelletaan useisiin tyypillisiin ionosfäärin ilmiöihin. Tulokset osoittavat induktiivisten sähkökenttien ja virtojen olevan tärkeitä paikallisissa, erittäin nopeita ajallisia muutoksia sisältävissä tilanteissa (kuten länteen etenevä hyöky, WTS). Tällaisissa tilanteissa induktio voi paikallisesti tuottaa jopa 20-30% ionosfäärin sähkökentästä ja virroista. Induktio vaikuttaa myös ionosfäärin ja magnetosfäärin välillä kulkeviin magneettikentän suuntaisiin virtoihin, ja tätä kautta kyseisten alueiden väliseen vuorovaikutukseen.

Julkaisijayksikkö
Avaruus ja yläilmakehä

Luokitus (UDK)
52

Asiasanat
Ionosfääri, Sähkömagnetismi

ISSN ja avainnimike
0782-6117 Finnish Meteorological Institute Contributions

ISBN
978-951-697-632-0 (nidottu), 978-952-10-4243-0 (pdf)

Kieli
Englanti

Myynti
Ilmatieteen laitos / Kirjasto
PL 503, 00101 Helsinki

Sivumäärä 170

Hinta

Lisätietoja

Preface

This thesis work has been done at the Space Research Unit (AVA) of the Finnish Meteorological Institute during years 2003-2007. I would like to use this opportunity to thank my supervisors Dr. Olaf Amm (the official one) and Dr. Ari Viljanen (the inofficial one) for their guidance. I also thank my colleagues at AVA for interesting discussions, especially during the coffee breaks.

I have been financially supported by the national Graduate School in Astronomy and Space Physics during years 2003-2007 and by the Acadmy of Finland project 115947 during year 2007. Additionally, I have received travel support for attending several conferences and workshops from Vilho, Yrjö and Kalle Väisälä foundation, Magnus Ehrnrooth foundation, Chancellor of the University of Helsinki and Sohlberg's delegation.

Helsinki, September 2007
Heikki Vanhamäki

Contents

Notation

$\boldsymbol{B}$	Magnetic field
$\boldsymbol{B}_G$	Magnetic field at the ground surface
$\boldsymbol{E}$	Electric field
$\boldsymbol{E}^{pot}$	Potential electric field
$\boldsymbol{E}^{ind}$	Induced electric field
$\tilde{\boldsymbol{E}}$	Fourier transform of $\boldsymbol{E}$ (others in similar fashion)
$\boldsymbol{j}$	Current density
$j_\parallel$	Field-aligned current density
$\boldsymbol{J}$	Surface current density
$\boldsymbol{J}_{eq}$	Equivalent current density
$\boldsymbol{J}_{CF}$	Curl-free part of current density
$\boldsymbol{J}_{DF}$	Divergence-free part of current density
$\boldsymbol{J}^{cf}$	Curl-free elementary current system
$\boldsymbol{J}^{df}$	Divergence-free elementary current system
σ_H, σ_P	Hall and Pedersen conductivities
Σ_H, Σ_P	Hall and Pedersen conductances
$\hat{\boldsymbol{e}}_x$, $\hat{\boldsymbol{e}}_y$, $\hat{\boldsymbol{e}}_z$	Cartesian unit vectors
$\hat{\boldsymbol{e}}_\perp$, $\hat{\boldsymbol{e}}_\parallel$	Unit vectors perpendicular and parallel to the background $\boldsymbol{B}$

List of acronyms

ASC	All-sky camera
CECS	Cartesian elementary current system
CF	Curl-free
DF	Divergence-free
EISCAT	European Incoherent Scatter
FAC	Field-aligned current
IMAGE	International Monitor for Auroral Geomagnetic Effects
MHD	Magnetohydrodynamics
MIRACLE	Magnetometers - Ionospheric Radars- Allsky Cameras Large Experiment
SECS	Spherical elementary current system
STARE	Scandinavian Twin Auroral Radar Experiment
SuperDARN	Super Dual Auroral Radar Network
WTS	Westward traveling surge

Summaries of the original publications

This thesis consist of an introductory part and the following five research articles:

PAPER I

Vanhamäki H., O. Amm and A. Viljanen, "One-dimensional upward continuation of the ground magnetic field disturbance using elementary current systems", *Earth, Planets and Space*, **55**, 613–625, 2003.

This paper presents a new version of the elementary current method for determining ionospheric equivalent currents. In the new method ionospheric currents are assumed to be 1-dimensional (only meridional variations), so that measurements from just a single meridional chain of magnetometers are needed. In contrast to previous models, the new 1D SECS method takes spherical geometry into account. The new method is compared against an earlier 1-dimensional analysis method based on Fourier-transform. We conclude that the 1D SECS method is superior to the earlier approach.

PAPER II

Vanhamäki H. and O. Amm, "A new method to estimate ionospheric electric fields and currents using data from a local ground magnetometer network", *Ann. Geophys.*, **25**, 1141–1156, 2007.

In Paper II we present a new formulation of the traditional KRM method. The task is to determine the ionospheric electric field and currents using ground magnetic measurements and ionospheric conductances as input data. Our formulation is based on the elementary current systems, and it differs from the traditional KRM method both in the mathematical approach and in the numerical solution algorithm. These new features make our calculation method well suited for local studies, where the traditional KRM formulation is error-prone due to a strong dependence on (unknown) boundary conditions. This is demonstrated in several model situations.

PAPER III

Vanhamäki H., A. Viljanen and O. Amm, "Induction effects on ionospheric electric and magnetic fields", *Ann. Geophys.*, **23**, 1735–1746, 2005.

This paper contains our first estimates of the role of inductive effects in ionospheric electrodynamics. We estimate both the ionospheric self-induction (primary process) and ionospheric effects of ground induction (secondary process). Our results are quite approximative, and should be considered as order of magnitude estimates. Nevertheless, we can conclude that ionospheric self-induction may produce significant electric fields in some situations. Inductive coupling between the ionosphere and solid earth does not seem to produce significant effects in ionospheric electric fields, but it does affect the magnetic field measurements by low-orbit satellites.

PAPER IV

Vanhamäki H., O. Amm and A. Viljanen, "New method for solving inductive electric fields in the non-uniformly conducting ionosphere", *Ann. Geophys.*, **24**, 2573–2582, 2006.

Here we present a new way of calculating induced electric fields in the ionosphere. With the new method the induced electric field is calculated self-consistently, in contrast to approximative methods used in Paper III. The new method is validated by comparing it with previous results of Alfvén wave reflection from the ionosphere. In contrast to previous approaches, the input parameters of the new method can be obtained from ground-based measurements.

PAPER V

Vanhamäki H., O. Amm and A. Viljanen, "Role of inductive electric fields and currents in dynamical ionospheric situations", *Ann. Geophys.*, **25**, 437–455, 2007.

In this paper we apply the method developed in Paper IV to several typical ionospheric phenomena. We conclude that ionospheric self-induction plays an important role in the most dynamical ionospheric situation, like in the westward traveling surge. Induction affects not only the ionospheric electric field, but also the field aligned currents and ionosphere-magnetosphere coupling.

In Papers I-V the author wrote main parts of the text, with factual and editorial assistance from the co-authors. In Papers I and III the author carried out the study following outlines given by the co-authors. In Papers II, IV and V the co-authors acted as supervisors, while the author was responsible for inventing the new theoretical methods as well as planning and performing the practical work.

Chapter 1

Introduction

This thesis deals with theoretical approaches in modeling ionospheric electrodynamics. In the research Papers I-V we have concentrated on two main themes: Development of new data-analysis techniques and study of inductive phenomena in the ionospheric electrodynamics. Several different data analysis techniques are needed in ionospheric research, in order to extract relevant information from the different sets of measurements that are available. The new techniques developed in this thesis improve the previous ways of obtaining ionospheric currents and electric fields from ground magnetic measurements. In the past it has been usually assumed that inductive phenomena are negligible in the ionosphere. This assumption is used in many data analysis methods, because the analysis can be simplified by representing ionospheric electric field in terms of a potential. However, recently it has been realized that in some situations inductive phenomena may play an important role in ionospheric electrodynamics. The development of new calculation techniques for induction studies and their application to different ionospheric phenomena forms the second part of the thesis. The two lines of study are connected by a common mathematical technique, the use of elementary current systems (ECS), that are a set of special vector basis functions for representing 2-dimensional vector fields.

In this introductory part we provide a background for the studies performed in Papers I-V, and connect them to other research activities in the field of ionospheric physics. We begin by giving a brief overview of the near Earth space environment and discuss the electric properties of the ionosphere in Sections 1.1 and 1.2. Several different experimental techniques and theoretical methods have been developed over the years for ionospheric studies. In Chapter 2 we review some of these methods, as well as some models of typical ionospheric phenomena. In Chapter 3 we discuss the new data-analysis techniques introduced in Papers I and II. Ionospheric self-induction and the inductive coupling between the ionosphere and solid earth were studied in Papers III-V, and are discussed further

in Chapter 4. Chapter 5 is conclusions and outlook. In Appendix A we summarize some properties of the Cartesian elementary current systems (CECS), that form a central part of the numerical methods used in the thesis.

1.1 Ionosphere and near Earth space environment

The ionosphere is the upper part of the atmosphere, where a significant fraction of the gas is ionized. Solar ultraviolet (UV) radiation and energetic particle precipitation from the magnetosphere are the main ionizing agents. Some ionization is also caused by solar X-rays and energetic particles together with galactic cosmic rays. The level of ionization depends not only on the production of electron-ion pairs, but also on the rate of recombination and different transport phenomena (see e.g. Schunk and Nagy, 2000).

The ionosphere is often considered to consist of several layers, that have different electrodynamic properties. Figure 1.1 illustrates typical daytime and nighttime electron density profiles at high latitudes. The density of free electrons has a maximum at about 200-450 km altitude, and the region around this maximum is called the F-layer. The typical density of free electrons in the F-layer is $10^{12}\ \mathrm{m}^{-3}$, which means that only about 0.1-1% of the gas is ionized. However, even this ionization fraction is enough to turn the gas into plasma, where collective electromagnetic phenomena affect the behavior of the gas in a significant manner. Above the F-layer density maximum the high-latitude auroral ionosphere merges with the magnetosphere without any clear upper boundary. Below the F-layer there is often a secondary maximum of the electron density in the E-layer, at about 90-140 km altitude. In the auroal regions large electric currents may flow in the E-layer, and therefore our main attention will be in this region. Below the E-layer, at 50-90 km altitude, there is still a weakly ionized D-layer that is usually present only during day time. It should be noted that the ionospheric electron density is highly variable. There are more or less regular seasonal and diurnal cycles, together with a roughly 11-year cycle associated with the solar activity. The daily variations at high latitudes are illustrated in Fig. 1.1. During night photoionization by solar radiation stops, and recombination decreases the density of free electrons. Additionally, at the auroral regions magnetospheric particle precipitation shows large spatial and temporal variations, which may lead to significant enhancements in the ionospheric electron density.

It is impossible to discuss ionospheric physics without some discussion about the magnetosphere and solar wind. The magnetosphere is formed when the solar wind interacts with the Earth's magnetic field. The magnetized plasma forming the solar wind cannot freely move across magnetic fields, so the Earth's field forms an obstacle around which the solar wind flows. The solar wind deforms the Earth's

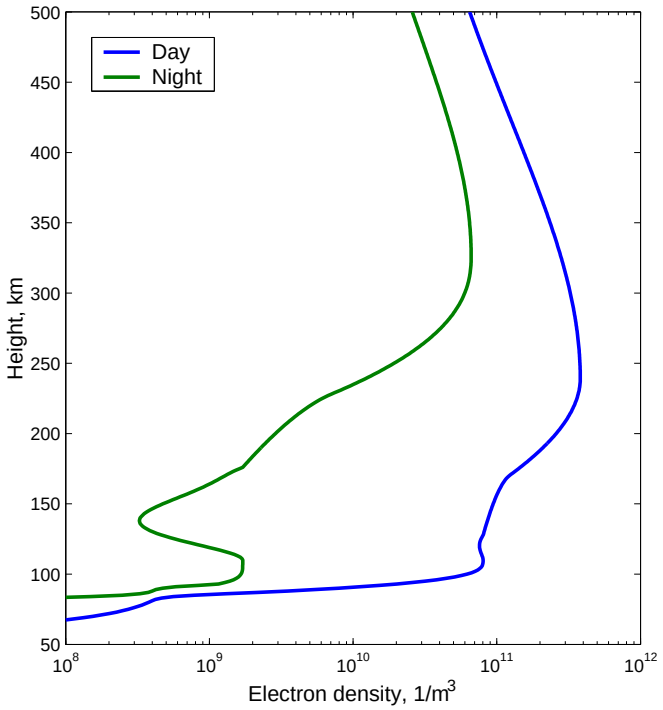

Figure 1.1: Typical height profiles of the ionospheric electron density for local noon and midnight above Helsinki. Profiles are from the international reference ionosphere (IRI) 2001 model, calculated for 1.3.2007 using solar and geomagnetic activity levels appropiate for that day. IRI is described by Bilitza (2001) and the computer code is available at [1].

dipolar magnetic field by compressing it in the day side and stretching it into a long tail in the night side, as schematically shown in Fig. 1.2. This deformation creates large current systems inside the magnetosphere, and part of these currents flow along magnetic field lines into (or out of) the polar ionospheres (e.g. Cowley, 2000). The solar wind exhibits large variations in speed, density and ambient magnetic field, and these changes affect the energy transport from the solar wind to the magnetosphere (e.g. Palmroth, 2003). Consequently, changes in the solar wind affect also the magnetospheric and ionospheric current systems, and may result in geomagnetic storms and other disturbances, as discussed in Section 2.3. The most readily observed result of this interaction chain are the aurorae, which are created when high-energy particles injected from the magnetosphere collide with atmospheric particles.

In addition to the magnetospheric connection, the ionosphere also interacts

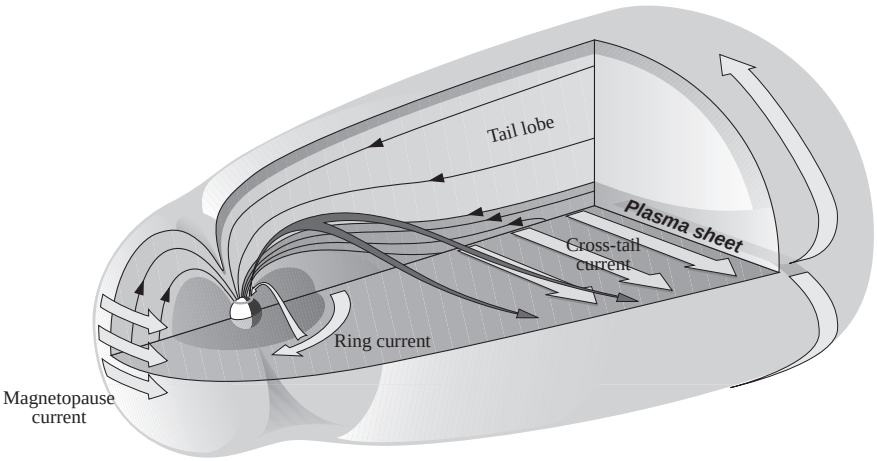

Figure 1.2: Schematic presentation of the Earth's magnetosphere and its most important current systems. Illustration by Teemu Mäkinen.

with the neutral atmosphere. The neutral and charged components interact through particle collisions, which decrease rapidly with altitude. The far more massive neutral gas provides background composition and a heat sink to the ionosphere. Magnetospheric particle precipitation and Joule heating by ionospheric currents heat the upper atmosphere, modifying the wind patterns and also the ion composition (Schunk and Nagy, 2000). These heating mechanisms are enhanced during geomagnetic storms and substorms, when large amounts of energy are transported from the solar wind to the magnetosphere-ionosphere system. The neutral wind dynamo driven by thermospheric winds also affects the ionospheric electric fields and currents (e.g., Richmond, 1989). For example, on magnetically quiet days the neutral wind dynamo (driven by solar radiation) is responsible for the solar quiet (Sq) current system in the ionosphere (e.g., Campbell, 1989). The large mass of the neutral gas also enables a flywheel effect: An intense geomagnetic storm transfers momentum into the high latitude neutral atmosphere, and after the storm the enhanced convection drives the neutral wind dynamo for several hours (Lyons et al., 1985).

Above we have given a very short overview of the near-Earth space environment, together with some references on more specific topics. Broader textbooks on the above subjects are e.g. Schunk and Nagy (2000) on the ionosphere, Ohtani et al. (2000) on the magnetosphere and ionosphere-magnetosphere coupling as well as Parks (1991) and Baumjohann and Treumann (1997) on space physics in general. Paschmann et al. (2002) give an extensive review of auroral phenomena in the high latitude ionosphere and related magnetospheric processes. The English

version of the free encyclopedia Wikipedia [2] has several introductory articles on space physics. Also the Oulu Space Physics Textbook [3] features several introductory texts, together with more detailed articles on various topics.

1.2 Electric fields and currents in the ionosphere

In this section we give a brief introduction to the main aspects of ionospheric electrodynamics. A more thorough introduction is given e.g. by Richmond and Thayer (2000) and Paschmann et al. (2002). As mentioned above, ionospheric electric currents are concentrated in the E-layer. To a good approximation the ionospheric Ohm's law, relating the electric field $\boldsymbol{E}$ and current density $\boldsymbol{j}$, can be written as

$$\boldsymbol{j} = \sigma_P \boldsymbol{E}_\perp + \sigma_H \hat{\boldsymbol{e}}_\parallel \times \boldsymbol{E}_\perp + \sigma_\parallel \boldsymbol{E}_\parallel. \tag{1.1}$$

The electric field is divided into two parts, $\boldsymbol{E}_\perp$ perpendicular to the background magnetic field and $\boldsymbol{E}_\parallel$ parallel to it. The ionospheric conductivity tensor consists of three elements, Pedersen conductivity σ_P along $\boldsymbol{E}_\perp$, Hall conductivity σ_H along $\hat{\boldsymbol{e}}_\parallel \times \boldsymbol{E}_\perp$ and field aligned conductivity $\sigma_\parallel$ in the direction of the magnetic field.

The different conductivities appearing in Eq. (1.1) can be derived from the motion of the individual particles in external electric and magnetic fields (e.g. Parks, 1991). The Pedersen and Hall conductivities depend mostly on the electron density and collision frequencies between charged and neutral particles. Above the E-layer the gas density is so low that the collision frequencies are negligible, which results in very low conductivities σ_P and σ_H. In this region the electrons and ions move under the $\boldsymbol{E} \times \boldsymbol{B}$ drift (e.g. Baumjohann and Treumann, 1997), without carrying any net current. Below the E-layer the conductivities decrease rapidly, as the electron density drops and both ions and electrons become collision dominated. Between these two regimes, where there are enough free charges to carry the current and also a sufficient number of collisions to disrupt the drift, the Pedersen and Hall conductivities have a maximum. Figure 1.3 shows typical altitude profiles of the conductivities.

The altitude range where the perpendicular conductivities σ_P and σ_H are near their maximum values is only about 20-50 km wide. This is a rather narrow region, when compared with the total extent of the ionosphere. For this reason it is common to use a thin-sheet approximation, where we assume that the horizontal currents flow at a thin spherical shell at some fixed altitude. If we assume that the electric field varies much more slowly with altitude than the conductivities, we may write the height-integrated horizontal part of Ohm's law as

$$\boldsymbol{J} = \Sigma_P \boldsymbol{E}_\perp - \Sigma_H \hat{\boldsymbol{e}}_r \times \boldsymbol{E}_\perp. \tag{1.2}$$

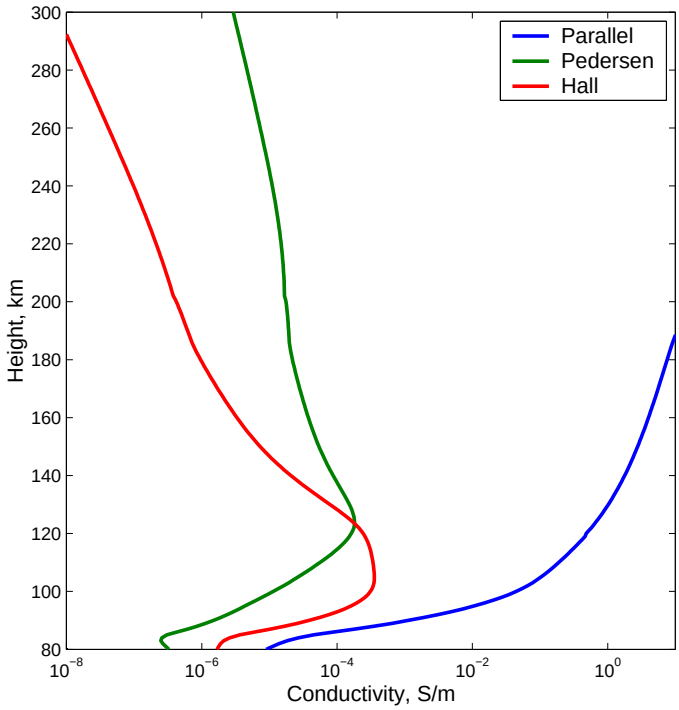

Figure 1.3: Typical altitude profiles of the ionospheric Pedersen and Hall conductivities together with the field aligned conductivity. These profiles correspond (roughly) to the daytime electron density profile in Fig. 1.1. Conductivities were calculated with a model provided by [4].

Here $\boldsymbol{J}$ is the horizontal sheet current density and the Hall and Pedersen conductances are defined as

$$\Sigma_{\binom{P}{H}} = \int_{E-layer} \sigma_{\binom{P}{H}} \, \mathrm{dz}.$$

Furthermore, in Eq. (1.2) we have made the frequently used assumption of a radial magnetic field by replacing $\hat{\boldsymbol{e}}_{\parallel}$ with $-\hat{\boldsymbol{e}}_r$ (minus sign is for northern hemisphere). This assumption is exactly valid only at the magnetic poles. Elsewhere the inclination of the field affects the Hall and Pedersen conductivities in Eq. (1.2). The necessary modifications have been studied e.g. by Amm (1998), who concluded that the effects are small with inclinations $\chi > 70^{\circ}$. Another commonly used approximation is to neglect the curvature of the ionosphere in small scales ($\lesssim 1000$ km), and use Cartesian instead of spherical geometry.

Charged particles are free to move along the magnetic field, but not across it. For this reason the field-aligned conductivity $\sigma_{\parallel}$ above the D-layer is many orders

of magnitude larger than σ_P or σ_H, as can be seen also in Fig. 1.3. Consequently, it is often assumed that the electric field $\boldsymbol{E}_\parallel$ parallel to the magnetic field vanishes, and instead of Ohm's law the parallel component of the current, $j_\parallel$, is given by current continuity,

$$j_\parallel = -\nabla \cdot \boldsymbol{J}. \tag{1.3}$$

Current continuity is a very good approximation, for typical ionospheric electric fields can be supported with just $\sim 10^{-13}$ C/m^2 surface charge densities[1]. This should be compared with typical FAC densities of $\sim$1 A/km^2, which gives a characteristic time scale of

$$\frac{|\text{surface charge}|}{|\text{FAC}|} \approx \frac{10^{-13}\text{C/m}}{1\text{A/km}^2} = 10^{-7}\,\text{s}. \tag{1.4}$$

So even small deviations from Eq. (1.3) would create large electric fields very quickly.

Large scale temporal variations in ionospheric current systems occur usually in time-scales of few minutes, or more. Therefore inductive effects are generally expected to be small, and another common assumption is to consider the electric field to be given by a potential,

$$\boldsymbol{E} = -\nabla\phi. \tag{1.5}$$

This is usually a valid assumption and it is a central part of many data-analysis methods, as discussed in Section 2.2. If we can assume that $E_\parallel = 0$ and Eq. (1.5) is valid, the magnetic field lines are equipotentials. This means that the electric field can be mapped along the magnetic field lines between ionosphere and different regions of the magnetosphere. However, the above conditions are not generally valid in the magnetosphere, and the mapping procedure is more complicated (see e.g. Toivanen et al., 1998). Moreover, in some very dynamical situations inductive effects may play a large part also in ionospheric electrodynamics, in which case Eq. (1.5) is no longer valid even in the ionosphere. We discuss ionospheric induction further in Papers III-V and in Section 4.

Here we have reviewed some general properties of ionospheric electric fields and currents, together with some commonly used approximations. Typical ionospheric phenomena are discussed in Section 2.3.

[1] Surface charge density can be calculated from the divergence of the electric field. See Untiedt and Baumjohann (1993) for a further discussion.

Chapter 2

Measurements, theory and models

In this chapter we first briefly review some of the most important measurement techniques used in the ionospheric research. In Section 2.2 we discuss some selected analysis methods, that are widely used to derive ionospheric electrodynamic parameters from ground or space based measurements. The new analysis methods developed in Papers I and II are discussed separately in Chapter 3. Finally in Section 2.3 we present an overview of typical ionospheric phenomena and models of some specific events based on measurements and data analysis. In Papers I-V we have tested the new data analysis methods and studied ionospheric induction using these models as examples of typical ionospheric phenomena.

2.1 Overview of selected measurement techniques

In order to get an accurate picture of ionospheric electrodynamics, we need to observe several different physical quantities with a good spatial and temporal resolution. This is most readily realized with large instrument networks, such as the MIRACLE network [5] illustrated in Fig. 2.1. MIRACLE consists of magnetometers, all-sky cameras (ASC) and radars situated in the northern Europe. Also various other instruments that are not part of the MIRACLE network operate in the same area (e.g. the EISCAT incoherent scatter radars [6] and SuperDARN radars [7]). In this section we will briefly describe some of these instruments. In addition to the various ground-based instruments described here, satellite measurements provide invaluable information about the magnetosphere-ionosphere system. Thorough discussions of combined ground and satellite-based observations are given e.g. by Paschmann et al. (2002) and Amm et al. (2005). Figure 2.2 is a schematic summary of the most important ionospheric electrodynamic parameters and the instruments used to measure them.

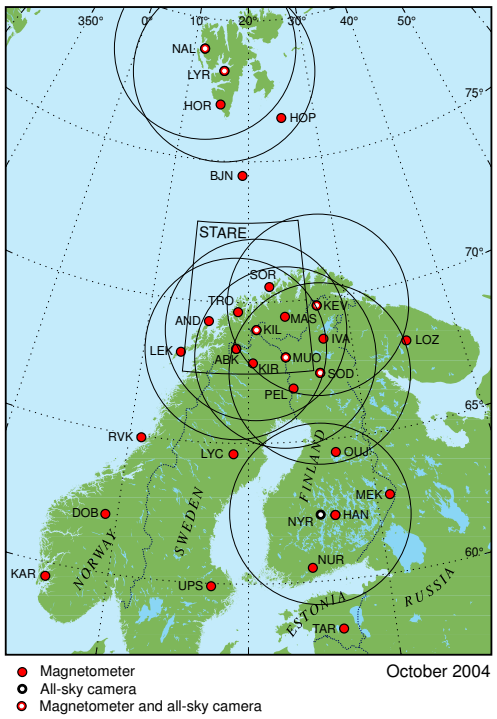

Figure 2.1: The MIRACLE instrument network (Magnetometers - Ionospheric Radars - Allsky Cameras Large Experiment, [5]). Circles give the field of view of each all sky camera. Also the combined field of view of the STARE radars (decommissioned in May 2005) is shown. Illustration by Lasse Häkkinen.

2.1.1 Magnetic measurements

Magnetometers are used to measure the magnetic variations produced by different current systems in the Earth and near space. Wide magnetometer networks, such as illustrated in Fig. 2.1, are used to monitor the geomagnetic activity almost globally. Data from different magnetometer stations is available e.g. at [8] or [9].

There are several different mechanisms that can be used as the operation principle of a magnetometer. One commonly used construction is the fluxgate magnetometer (e.g. Campbell, 1997). It consists of a primary drive coil and a secondary sense coil that are wound around a common core. AC current is fed to the drive coil, so that the core is saturated in each cycle. Even a weak external magnetic field parallel to the core axes will cause asymmetry in the saturation, so that the core saturates more easily in the direction of the external field. This asymmetry depends on the strength of the external field, and can be measured using the

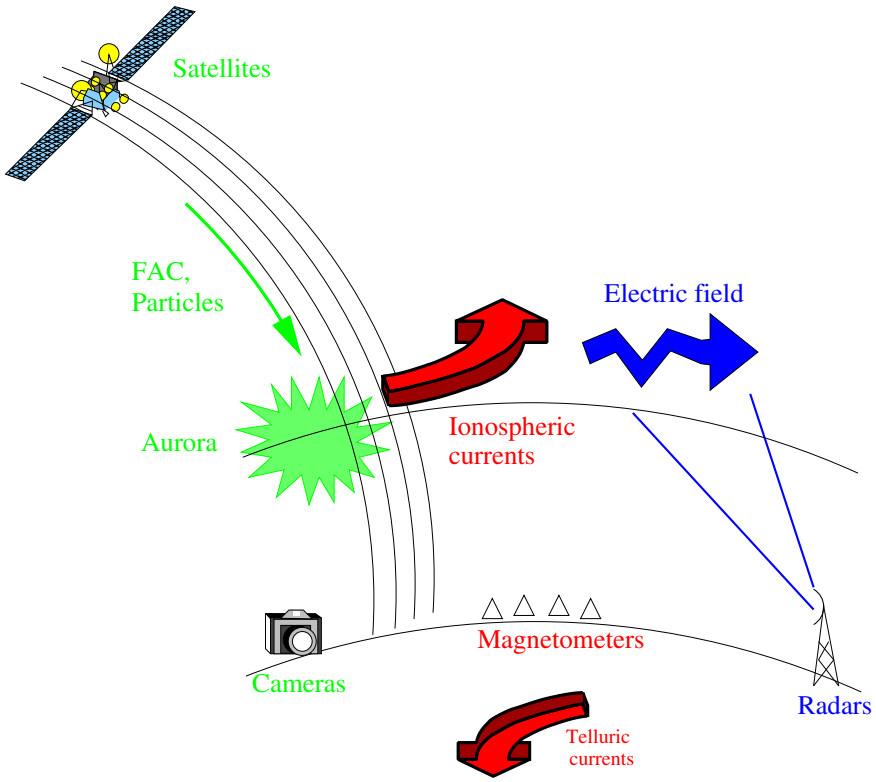

Figure 2.2: Different physical quantities relevant to ionospheric electrodynamics, and the instruments used to measure them.

secondary coil. Thus a fluxgate magnetometer is able to measure the vector components of the magnetic field, with accuracy up to 0.1 nT.

Different magnetic indices provide simple, quantitative estimates of ionospheric and magnetospheric activity. Perhaps the most widely used indices are the Dst and AE indices. The Dst index is mainly affected by the magnetospheric ring current and cross tail current (see Fig. 1.2). It is a measure of the global magnetospheric activity and is used to monitor development of geomagnetic storms (Section 2.3.1). The AE index, and the related AL and AU indices, are used to monitor auroral electrojet currents and substorm activity (Section 2.3.2) at high magnetic latitudes. The Dst and AE indices are constructed by taking the maximum instantaneous deviation from the quiet time base level at selected observatories around the world. The Dst index is based on measurements at four mid-latitude observatories, while 11 observatories near the northern auroral oval contribute to the the AE index. Dst, AE and other magnetic indices are available at [4], together

with further discussion and references. Different geomagnetic indices are also discussed by Mayaud (1980) and Gonzalez et al. (1994). More advanced techniques developed for analyzing magnetic data are discussed in Section 2.2 and 3.1, as well as in Paper I.

2.1.2 Measurements using radio waves

The ionosphere affects the propagation of radio waves that are transmitted through it. For example, at the HF band around 3-30 MHz the ionosphere reflects radio waves efficiently, enabling direct long distance radio communication. On the other hand, this means that radio waves can be used to measure various ionospheric parameters. A thorough discussion of radio wave propagation in the ionosphere is given e.g. by Davies (1996).

Ionosonde

Different ionospheric radars transmit radio pulses to the ionosphere and measure the reflected (or scattered) echo. Perhaps the simplest instrument of this kind is the ionosonde, which transmits short pulses with different frequencies directly upwards. The altitude where the pulses are reflected back to the ground depends on the transmission frequency and ionospheric electron density. As the electron density increases with altitude, higher frequencies are reflected at increasingly higher altitudes, until at some critical frequency the pulses are able to penetrate the F-layer density maximum and escape to space. From the echo times at different frequencies it is possible to calculate the ionospheric electron density as a function of altitude (e.g. Davies, 1996). Ionosonde data is available at [10].

Incoherent scatter radars

Incoherent scatter radars like EISCAT, [6], operate at higher frequencies than ionosondes. Instead of a nearly total reflection, only a small part of the transmitted power is scattered by thermal fluctuations in the ionospheric electron density, and can be received at the ground. Consequently, powerful transmitters and sensitive receivers with large antennas are required. From incoherent scatter radar measurements it is possible to estimate the ion flow speed in the line of sight direction, electron density, ion and electron temperature and other parameters with a good spatial resolution along the beam. Measurements can be done only in one specific direction at a time, although new radars that use phased antenna arrays are able to switch the beam direction very rapidly. An introduction to incoherent scatter radars and analysis of the measurements is given by Nygrén (1996).

Coherent scatter radars

Coherent scatter radars, such as the SuperDARN network ([7], Greenwald et al., 1995) and the STARE radars (Fig. 2.1, [5]), operate usually at the HF band. The radar signal is transmitted at low elevation angles, so that it travels almost horizontally in the ionosphere. Disturbances in the ionospheric electron density scatter the radio waves, reflecting part of the signal back to the transmitter. The Doppler shift in the received signals gives an estimate of the line of sight velocity of plasma, which can be converted into the electric field by assuming $\boldsymbol{E} \times \boldsymbol{B}$ drift. If two or more radars measure the plasma motion from different directions, 2-dimensional velocity and electric field distributions can be obtained. In global studies, gaps in the radar data are usually treated by fitting an electric potential model (parametrized on e.g. solar wind properties) into the data (Ruohoniemi and Baker, 1998).

Other instruments

In addition to radars, also other radio systems can be used in ionospheric studies. For example, riometers (e.g. Browne et al., 1995) are passive instruments that monitor steady galactic radio noise, and measure the variation of the signal strength caused by ionospheric absorption. Also the propagation delays in navigational signals transmitted by the GPS and other satellites may be used to monitor the variations of the electron density in the ionosphere (e.g. Nygrén at al., 2000; Jakowski et al., 2002; Kersley et al., 2005; Stolle at al., 2005).

2.1.3 All sky cameras

Auroras have been studied using optical images since the beginning of the 20th century. All-sky cameras (ASC) take images of the whole sky at some specific wavelengths (e.g. at 486, 558 and 630 nm) and also at the white light, usually every 10-30 seconds or so. The observational area of a single ASC is about 600 km in diameter (at about 110 km altitude), as illustrated in Fig. 2.1.

ASC images form a basis for classifying different auroral phenomena, such as arcs, spirals and Ω-bands, which are created by different processes in the magnetosphere-ionosphere system (Akasofu and Kimball, 1964). Machine vision methods have been developed for detecting different types of auroral forms from the huge ASC image data bases, see e.g. Syrjäsuo and Donovan (2004) and references therein. Images from ASC networks can also be used to reconstruct the energy flux of the precipitating particles (Janhunen, 2001; Partamies et al., 2004). The obtained energy fluxes and characteristic energies can (at least in principle) be used to estimate the ionospheric conductances (Robinson et al., 1987), which

Table 2.1: Table of different analysis methods, adapted from Amm et al. (2003). See Section 2.2 for details.

Input	Assumptions	Output	Name of method	Remarks
$\boldsymbol{B}_G$	-	$\boldsymbol{J}_{eq,ion}, \boldsymbol{J}_{eq,int}$	Field continuation and separation	No true currents, no FAC
$\boldsymbol{B}_G$, {$\boldsymbol{E}$, satellite data}	Σ_P, Σ_H $\nabla \times \boldsymbol{E} = 0$	{$\boldsymbol{E}$}, $\boldsymbol{J}$, $j_\parallel$	AMIE	Optimization method, also with sparse data
$\boldsymbol{B}_G$, $j_\parallel$, {$\boldsymbol{E}$}	-	$\boldsymbol{J}$, {Σ_p, Σ_H}	Elementary current method	
$\boldsymbol{B}_G$	Σ_P, Σ_H $\nabla \times \boldsymbol{E} = 0$	$\boldsymbol{E}$, $\boldsymbol{J}$, $j_\parallel$	KRM	Boundary conditions critical if non-global
$j_\parallel$	Σ_P, Σ_H $\nabla \times \boldsymbol{E} = 0$	$\boldsymbol{E}$, $\boldsymbol{J}$	-	Boundary conditions critical if non-global
$\boldsymbol{B}_G, \boldsymbol{E}$	$\alpha = \Sigma_H/\Sigma_P$	Σ_H, Σ_P, $\boldsymbol{J}$, $j_\parallel$	Method of characteristics ($\boldsymbol{J}_{eq}$-based)	α assesible from ASC or $\boldsymbol{B}_G$ data
$j_\parallel$, $\boldsymbol{E}$			(FAC-based)	

in turn are used as input in many analysis methods, as discussed in Section 2.2.

2.2 Overview of selected analysis methods

It is not always possible to measure directly those ionospheric parameters that we are most interested in. For example, magnetic measurements do not directly give the ionospheric currents, but instead we have to develop some theoretical framework so that we can estimate the currents from the magnetic disturbances they cause. In this thesis we are mostly interested in the electrodynamical parameters of the ionosphere, which are the electric field $\boldsymbol{E}$, horizontal currents $\boldsymbol{J}$, field aligned currents (FAC) $j_\parallel$ and conductances Σ_P and Σ_H. These quantities are not independent, as they are connected by Ohm's law (Eq. 1.2) and current continuity (Eq. 1.3). In some studies other parameters, like temperature and chemical composition, might be of interest.

Over the years several methods have been developed to estimate various parameters or their combinations from different sets of measured or modeled data. Here we discuss some of the most commonly used techniques. In papers I and II we developed two new analysis techniques, which will be discussed in more detail in Chapter 3. Table 2.1 gives an overview of selected analysis methods. The table is adapted from Amm et al. (2003), while also Untiedt and Baumjohann (1993) discuss most of these methods.

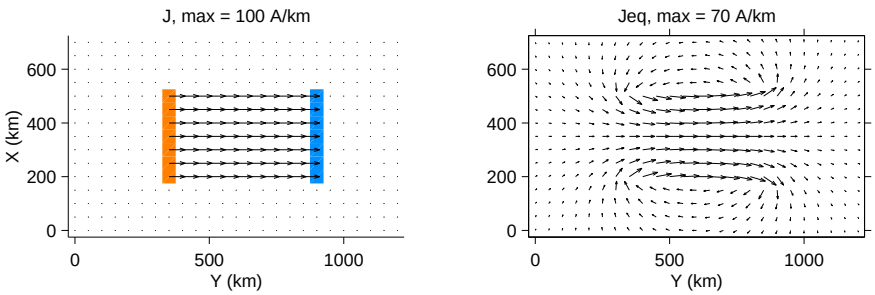

Figure 2.3: Example of a real ionospheric current distribution (left panel) and an equivalent current distribution (right panel) that produce the same magnetic field below the ionosphere. On the left panel upward FAC are marked in blue and downward FAC in red.

2.2.1 Equivalent currents from magnetic measurements

The ground magnetic data $\boldsymbol{B}_G$ is most conveniently used in form of ionospheric equivalent currents $\boldsymbol{J}_{eq,ion}$. By definition, ionospheric equivalent currents are divergence-free horizontal sheet currents, that produce the same magnetic field below the ionosphere as the real (unknown) 3-dimensional current system. Only the equivalent currents can be determined using ground magnetic measurements alone. Some additional data on ionospheric conductances, FAC or electric field is needed in order to determine the real 3-dimensional current system. In addition to external ionospheric and magnetospheric currents, there are also internal sources of magnetic disturbances due to induced currents in the Earth. They can be represented in terms of internal equivalent currents $\boldsymbol{J}_{eq,int}$. The measured ground magnetic field can be uniquely separated into internal and external parts (e.g. Pulkkinen et al., 2003b). The equivalent currents and various techniques to determine them are discussed separately in Section 3.1.

2.2.2 AMIE

One way of solving the ionospheric parameters is "trial and error" analysis, where distributions of conductivities, electric field etc. are varied, until a satisfactory agreement with observations is achieved (Untiedt and Baumjohann, 1993). In a way, the AMIE procedure (Assimilative Mapping of Ionospheric Electrodynamics, introduced by Richmond and Kamide, 1988) is an objective way of doing the optimization in a least squares sense. In AMIE different types of measurements are assimilated, together with some statistical models. This means that AMIE is very flexible, and can make use of sparse data sets that cover only a part of the

analysis region. AMIE requires the ionospheric Pedersen and Hall conductance distributions as input. In practice these are quite difficult to obtain from direct measurements, and typically some statistical models (perhaps modified by local measurements) are used (e.g. Richmond et al., 1988; Lu et al., 2001).

2.2.3 Elementary current method

If the ground magnetic field $\boldsymbol{B}_G$ and FAC are known, the horizontal ionospheric current density $\boldsymbol{J}$ can be calculated: Equivalent currents give the curl of the true currents as in Eq. (2.3), and FAC give the divergence according to Eq. (1.3). If $\nabla \times \boldsymbol{J}$ and $\nabla \cdot \boldsymbol{J}$ are known globally, $\boldsymbol{J}$ is uniquely determined. If data is available only in some limited region the solution is not unique, for a Laplacian field with zero curl and divergence inside the analysis area can be added to it. The solution for $\boldsymbol{J}$ is most readily obtained using the elementary current systems introduced by Amm (1997) (see also Appendix A). In this elementary current method, developed by Amm (2001), the ionospheric current is obtained directly from the data, without any assumed parameters. If also measurements of the electric field are available (e.g. from radars), the ionospheric conductances are obtained from Eq. (1.2).

2.2.4 KRM and method of characteristics

The three methods in the bottom of Table 2.1 are related to each other. From Ohm's law Eq. (1.2) one obtains the following expressions for the curl and divergence of the ionospheric current

$$\begin{aligned}(\nabla \times \boldsymbol{J})_z = {} & (\nabla \Sigma_P \times \boldsymbol{E})_z + \Sigma_P (\nabla \times \boldsymbol{E})_z + \nabla \Sigma_H \cdot \boldsymbol{E} + \\ & + \Sigma_H \nabla \cdot \boldsymbol{E}\end{aligned} \tag{2.1}$$

$$\begin{aligned}j_{\parallel} = {} & \nabla \Sigma_P \cdot \boldsymbol{E} + \Sigma_P \nabla \cdot \boldsymbol{E} - (\nabla \Sigma_H \times \boldsymbol{E})_z - \\ & - \Sigma_H (\nabla \times \boldsymbol{E})_z\end{aligned} \tag{2.2}$$

Here we have used the Cartesian coordinate system, but in global studies these equations are written in the spherical coordinate system. As explained in Section 3.1.2, at high magnetic latitudes we may approximate

$$(\nabla \times \boldsymbol{J})_z = (\nabla \times \boldsymbol{J}_{eq})_z \,. \tag{2.3}$$

This means that the curl of the real horizontal current system can be determined directly from ground based magnetic measurements. Equations (2.1)-(2.3) are used as the starting point in many analysis methods, which differ mainly in the assumptions on available data.

KRM

The KRM method (named after Kamide, Richmond and Matsushita) was introduced by Kamide et al. (1981). In the KRM method the ionospheric equivalent currents and ionospheric conductances are assumed to be known. If the ionospheric electric field is assumed to be given by a potential, as in Eq. (1.5), then Eqs. (2.1) and (2.3) give a second order partial differential equation for the potential. In global or hemispheric studies this equation can be integrated straightforwardly, but in regional scales boundary conditions for the potential are problematic (Murison et al., 1985). Also conductance distributions are difficult to obtain from measurements, so statistical models are commonly used. In Paper II we present a different formulation of the KRM problem, together with a new numerical technique based on the elementary current systems. The original KRM method and our new formulation are further discussed in Section 3.2.

"FAC-based KRM"

We can obtain a sort of FAC based KRM method from Eq. (2.2), if instead of equivalent currents the FAC are known (the unnamed method in Table 2.1). Also in this method the conductances are assumed to be known and the electric field is given by a potential. The use of the method is limited by the availability of global FAC measurements, and in smaller scales boundary conditions are a problem, as in the KRM. For example Rich and Kamide (1983) have used the method with statistical FAC and conductivity models, while some further references are given in Untiedt and Baumjohann (1993). Also global magnetospheric magnetohydrodynamic simulations usually solve the ionospheric current systems in this manner (Janhunen, 1998).

Method of characteristics

The method of characteristics was introduced by Inhester et al. (1985) for local studies in the Cartesian geometry. It was later generalized by Amm (1998) for the spherical geometry. In the method of characteristics the input quantities are the ionospheric electric field, equivalent currents and the conductance ratio $\alpha = \Sigma_H/\Sigma_P$. The electric field may be non-potential, so that $\nabla \times \boldsymbol{E} \neq 0$. With these known input parameters, Eq. (2.1) forms a first order partial differential equation for the Hall conductance Σ_H, which is solved by integration along the characteristic lines of the equation (hence the name of the method). The conductance ratio α is much easier to estimate than the conductances themselves (Lester et al., 1996; Ahn et al., 1998). Amm (1995) also concluded that the calculation method is not very sensitive to errors in α. The integration process begins from the boundaries of the calculation area, where boundary values for Σ_H must be

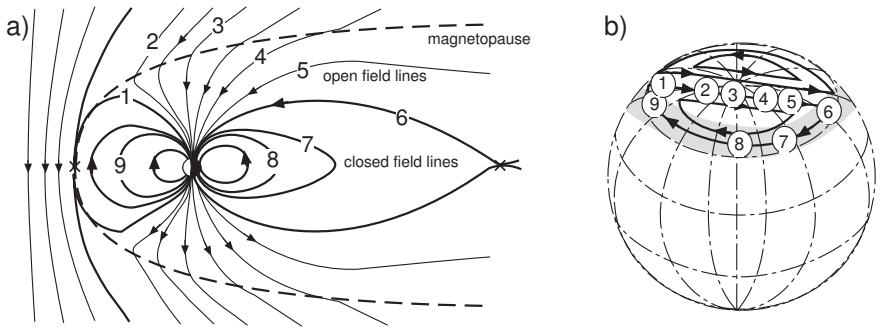

Figure 2.4: Schematic presentation of the magnetospheric and ionospheric convection during a southward IMF. Numbers in the left panel follow the flow of the magnetic field from the dayside magnetopause to the magnetotail and back. The right panel shows the corresponding convection in the polar ionosphere. Illustration by Minna Palmroth, after Dungey (1961).

assumed. However, the effect of different boundary conditions on the solution is usually not significant, and the affected areas can be identified. Further details and application examples are given by Inhester et al. (1985), Untiedt and Baumjohann (1993) and Amm (1995, 1998). There is also a FAC-based version of the method of characteristics, introduced by Amm (2002). In this version the equivalent currents are replaced by FAC in the input data set, and Eq. (2.2) is used instead of Eq. (2.1).

2.3 Typical ionospheric phenomena and models used in the thesis

As described in Section 1.1, ionospheric activity is to a large extent controlled by the solar wind and its interaction with the magnetosphere. Even during quiet, steady conditions the magnetosphere is heavily deformed by the solar wind, as illustrated in Fig. 1.2. The solar wind transfers energy and momentum into the magnetosphere, setting the plasma into convective motion. This convection is mapped to the ionosphere along the magnetic field, so that ionospheric convection forms a two-cell pattern around geomagnetic poles (Cowley, 2000). The main flow is across the polar cap from noon towards midnight, and the return flow takes place at lower magnetic latitudes. When the interplanetary magnetic field (IMF) in the solar wind points southward, reconnection at the sunward part of the magnetopause leads to efficient energy and plasma transport to the magnetosphere (e.g.

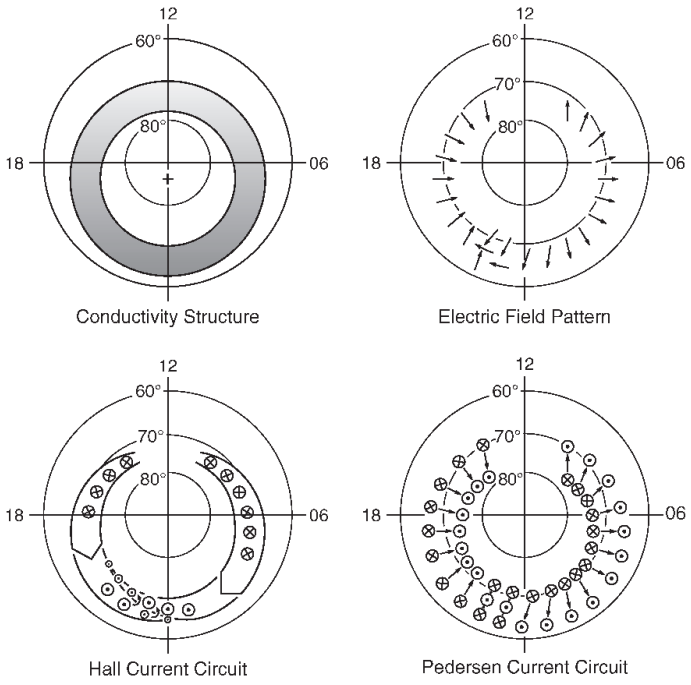

Figure 2.5: Schematic presentation of the average auroral current system. From Baumjohann and Treumann (1997)

Palmroth, 2003). This situation is illustrated in Fig. 2.4. The enhanced energy transfer to the magnetosphere may lead to increased magnetic activity, such as magnetic storms and substorms discussed below. The real ionospheric convection pattern is of course quite complicated. This can be seen from real-time convection maps obtained with the SuperDARN network, available at [7].

A part of the magnetospheric currents illustrated in Fig. 1.2 is connected to the polar ionospheres, and also the large scale magnetospheric convection electric field is mapped to the ionosphere along the field lines (Cowley, 2000). Together these imposed currents and electric fields create a large scale current system in the auroral ionosphere, as illustrated in Fig. 2.5. The ionospheric Pedersen and Hall conductances are enhanced in the auroral oval due to the energetic (some tens of keV) particle precipitation. The main ionospheric current system consists of an eastward electrojet in the evening sector and a westward electrojet in the morning sector. The FAC system is dominated by Region 1 and Region 2 currents (Iijima, 2000), which are situated at the poleward and equatorward edges of the oval, respectively.

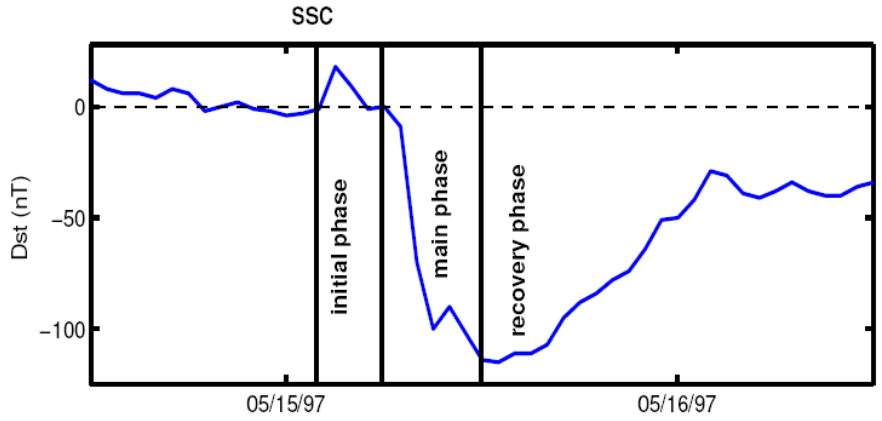

Figure 2.6: The Dst index and the different phases of the magnetic storm that occured on May 15-16, 1997. Figure is provided by Emilia Huttunen.

2.3.1 Geomagnetic storms

Geomagnetic storms are global magnetic disturbances that typically last 1-3 days, sometimes even longer (Gonzalez et al., 1994). Storms are caused by solar eruptions, like flares and coronal mass ejections, or high speed streams from coronal holes. These create shock waves and pressure pulses in the solar wind, that reach the Earth orbit in a few days. A geomagnetic storm often begins with a sudden storm commencement (SSC), which is seen as a few tens of nT increase in the Dst index (described in Section 2.1.1). The increase is caused by the sudden compression of the magnetosphere and the consequent increase of the magnetopause current, as the solar wind pressure pulse arrives. The main phase of the storm begins some tens of minutes later, when enhanced energy transfer from the solar wind starts to intensify magnetospheric current systems. This is seen as a strong decrease in the Dst index, which may drop well below -100 nT during intense storms (Gonzalez et al., 1994). The recovery phase begins when the solar wind energy input decreases, and the Dst index starts to slowly increase. Figure 2.6 shows the evolution of the Dst index during the different phases of a magnetic storm that occured on May 15-16, 1997.

Not all shock fronts or pressure pulses that hit the Earth's magnetosphere cause geomagnetic storms. The most important factor in the geoeffectiveness of different solar wind structures is the IMF orientation, as was demonstrated by Gonzalez and Tsurutani (1987). A southward IMF enables magnetic reconnection at the sunward magnetopause, making energy transport into the magnetosphere more efficient. During northward IMF orientation reconnection is weaker and takes place

at the flanks of the magnetosphere. Different drivers of magnetospheric storms are discussed by Huttunen (2005), while Huttunen et al. (2002) give a thorough discussion of the whole chain of events from the Sun to the ionosphere for a large storm in April 2000.

2.3.2 Substorms

Substorms are the other main class of large scale magnetic disturbances. In the magnetosphere substorms are seen as large scale reconfigurations of the current systems in the magnetotail, releasing energy and accelerating particles to high energies. Charged particles are precipitated to the nightside polar ionospheres, where an auroral substorm is observed (Akasofu, 1964). Substorms last typically $\sim$2 hours, and consist of three distinct stages: growth, expansion and recovery phases (McPherron, 1970).

The growth phase usually begins with a southward turning of the IMF. During this phase solar wind energy is loaded into the magnetosphere, which leads to an intensification of magnetospheric and ionospheric current systems. Intensification of the auroral electrojets is seen as an increase in the AE index (see Section 2.1.1). The growth phase ends with the onset of the expansion phase, which may be triggered by changes in the solar wind or by internal magnetospheric dynamics. In the ionosphere this is seen as a rapid poleward expansion of bright auroras, beginning near the local midnight. In the magnetosphere part of the cross tail current (see Fig. 1.2) is diverted to flow through the ionosphere, forming the substorm current wedge (SCW, McPherron et al., 1973). The SCW consists of an earthward (downward) FAC on the eastern side of the wedge, a westward ionospheric electrojet and an tailward (upward) FAC on the western side. This intensifies the auroral electrojet, so that ground magnetic variations may reach several thousand nT during the most intense substorms. Figure 2.7 shows the average behavior of the north-component of the ground magnetic field during a substorm. Also high speed plasma flows are created and particles are accelerated to high energies in the magnetosphere. During the expansion phase the magnetospheric magnetic field becomes more dipolar, relaxing from the stretched shape created during the growth phase. The expansion phase lasts $\sim$30 minutes, and is followed by the more gradual recovery phase. During the recovery phase auroral Ω-bands (see section 2.3.3), pulsating auroras and other dynamical features may be observed in the morning sector (Opgenoorth et al., 1994). The magnetosphere returns to the pre-substorm configuration, and the cross-tail current recovers. If conditions are favorable, another substorm cycle may begin.

Several different models for describing the magnetospheric dynamics during substorms have been suggested. These are discussed e.g. by Baker et al. (1996) and Lui (1996), while the relation between magnetic storms and substorms is

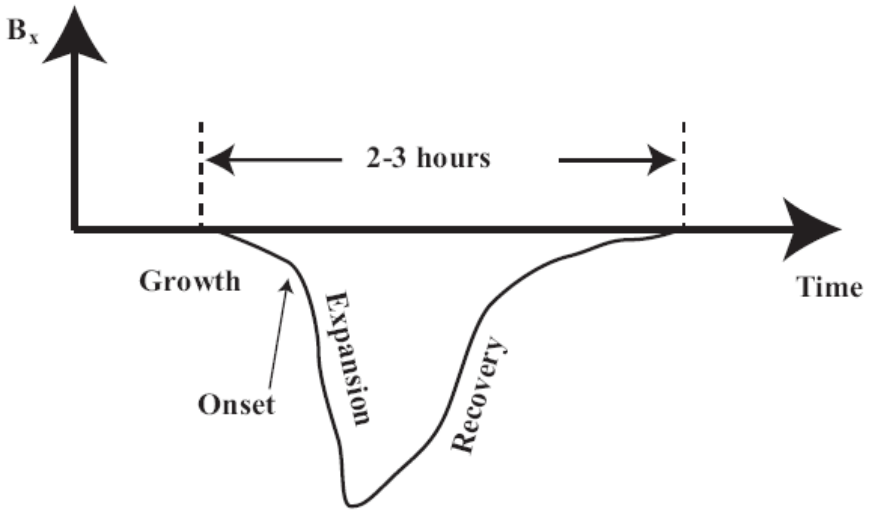

Figure 2.7: The average behavior of the north-component of the ground magnetic field during a substorm. Illustration by Mikko Syrjäsuo, after Kamide (1991).

considered e.g. by Gonzalez et al. (1994) and Sharma et al. (2004).

2.3.3 Models of some specific ionospheric systems

In this thesis we have used several data-based models of typical ionospheric current systems. In this section we give an overview of some of these models, and indicate their connection to the general ionospheric system described above. A far more thorough discussion is given e.g. by Untiedt and Baumjohann (1993) and Paschmann et al. (2002). The Ω-band and westward traveling surge (WTS) models that are used in Papers II, III and V have been constructed by Amm (1995) and Amm (1996). They are based on observational data obtained in northern Scandinavia by the Scandinavian Magnetometer Array, the EISCAT radar and the EISCAT magnetometer cross, and the STARE radar.

We concentrate on meso-scale phenomena, that have a spatial extent of a few hundred to a few thousand km. In these scales the Earth's curvature can be neglected, and we can use the Cartesian coordinate system, as in Papers II-V. The coordinate system is oriented so that the x-axis points to the North[1], y-axis to the East and z-axis vertically downward. The ionosphere is assumed to be the $z = 0$ plane, except in Paper III where the ground surface is $z = 0$ and ionosphere is $z = -110$ km.

[1]In our case towards geographical North. Also geomagnetic orientation could be used.

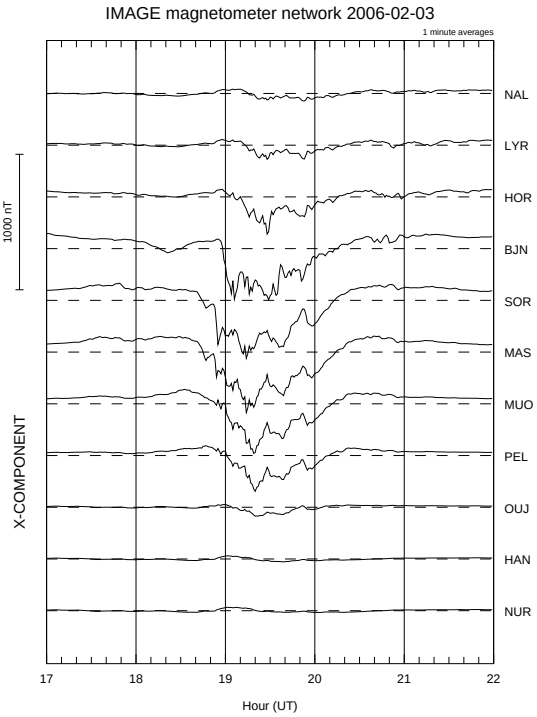

Figure 2.8: The X-component of ground magnetic disturbance created by a westward electrojet during otherwise quiet evening. The selected magnetometer stations form a North-South line across Scandinavia (see Fig. 2.1 for station locations).

Electrojets

Auroral electrojets are the most common current systems observed in the polar ionospheres. Figure 2.8 shows an example of ground magnetic disturbances associated with a westward electrojet flowing above the northern Scandinavia (see Fig. 2.1 for station locations).

Our model electrojets are oriented in the y-direction (East-West), and have a more or less Gaussian profile in the x-direction (North-South). For example, in the electrojet model of Paper II the ionospheric electric field points southward, as is the case for the morning side westward electrojet (see Fig. 2.5). The main electrojet current in this case is the Hall current flowing westward, while the Pedersen current flows in the x-direction and is connected to strips of oppositely directed FAC at the northern and southern edges of the electrojet.

In Papers I and V we use strictly one-dimensional electrojets, so that there is no variation in the y-direction. While this is an idealization, electrojets often have a nearly constant magnitude and direction over distances of a few thousand km (e.g. Untiedt and Baumjohann, 1993). In Paper V we use a model where an originally 1-dimensional electrojet starts to intensify at the western part, while the eastern part remains constant. During the intensification the electric field remains fixed, and only the conductances and currents vary. Our models are quite simplistic, but encompass the main electrojet features and agree qualitatively with results presented by Untiedt and Baumjohann (1993) and Amm (1995).

WTS

The westward traveling surge (WTS, Akasofu et al., 1965) is a substorm phenomenon that is observed in the evening sector after the substorm onset (Paschmann et al., 2002). The WTS is the westernmost part of the expanding auroral bulge that is created near the midnight sector in the substorm expansion phase. The surge moves westward with a velocity of 1-10 km/s, gradually slowing down as it propagates. Intense westward currents terminate at the "head" of the WTS, where FAC close the current back to magnetosphere. Electron precipitation increases the electric conductance in the head and wake of the WTS, while the electric field is suppressed there.

In Papers II, III and V we use a model of the WTS that encompasses the head and a part of the wake. In Papers III and V, where we study inductive effects, temporal variations are created by moving a snapshot model with a constant velocity. This is a reasonable approximation, for the WTS current system is often quite stationary in the co-moving reference frame (Untiedt and Baumjohann, 1993).

Ω-bands

Auroral Ω-bands are observed in the morning sector during the substorm recovery phase (Opgenoorth et al., 1994; Paschmann et al., 2002). They are quasi-periodic moving auroral structures that resemble the Greek letter omega (Akasofu and Kimball, 1964). The spatial extent of individual omegas is about 400-500 km, but the whole structure can cover several thousand km. Ω-bands usually drift eastward with a velocity of 0.4-2 km/s, often gaining speed with time. In the ground magnetic record the passage of Ω-bands is seen as Ps6 type magnetic pulsations (e.g. Untiedt and Baumjohann, 1993) with amplitudes varying from 10 to over 1000 nT. The oscillation time of the magnetic field is 5-40 minutes, corresponding to the drift velocity and separation of the individual omegas. Also Ω-bands are quite stationary in the moving reference frame, so temporal variations are created same way as in the WTS case.

Chapter 3

Equivalent currents and KRM: New methods for data-analysis

In this Chapter we review more thoroughly two of the data-analysis techniques mentioned in Table 2.1 and Section 2.2: Calculation of the equivalent currents from magnetic measurements and the KRM method. The reason for discussing these two cases in more detail is that in Papers I and II we present new results in these areas. In Section 3.1 we describe the concept of equivalent currents and various methods to determine them from magnetic measurements, among others the 1-dimensional elementary current method developed in Paper I. The KRM method and our new approach to the same problem are described in Section 3.2.

3.1 Magnetic measurements and ionospheric equivalent currents

As mentioned in Section 2.2.1, ionospheric equivalent currents $\boldsymbol{J}_{eq,ion}$ are defined as 2-dimensional, divergence-free sheet currents that produce the same magnetic field below the ionosphere as the real 3-dimensional current system. According to potential theory, this kind of equivalent current solution always exists and is uniquely defined.

In addition to external ionospheric and magnetospheric currents, there are also internal sources of magnetic disturbances. Magnetic variations caused by changes in external sources create an induced electric field, according to Faraday's law. The induced electric field drives currents in the ground, which depend also on the conductivity of the local bedrock. This process of geomagnetic induction distorts the original magnetic signal from external sources, and makes analysis more difficult (e.g. Rikitake and Honkura, 1985; Untiedt and Baumjohann, 1993). The magnetic variations that are caused by the internal sources can be represented

using internal equivalent currents $\boldsymbol{J}_{eq,int}$. These are analogous to $\boldsymbol{J}_{eq,ion}$, except that they produce the same magnetic field as the true ground induced currents above the Earth's surface.

3.1.1 Ionospheric equivalent currents

Here we give a simple derivation of the equivalent currents. In the neutral atmosphere between the ground surface ($z = h$) and ionosphere ($z = 0$), the magnetic field satisfies

$$\nabla \cdot \boldsymbol{B} = 0, \tag{3.1}$$

$$\nabla \times \boldsymbol{B} = 0. \tag{3.2}$$

Consequently, in this region it can be expressed in terms of a potential,

$$\boldsymbol{B} = -\nabla\psi, \tag{3.3}$$

so that

$$\nabla^2\psi = 0. \tag{3.4}$$

By taking Fourier-transform of the horizontal part of Eq. (3.4) we can represent the potential as a sum of plane waves. Each plane wave $\tilde{\psi}_{k_x,k_y}$ is of the form

$$\tilde{\psi}_{k_x,k_y}(z) = f(z)\, e^{-i(xk_x+yk_y)},$$

where k_x, k_y are the horizontal wavenumbers and function $f(z)$ describes the z-dependence. Eq. (3.4) gives

$$(\partial_z^2 - k_x^2 - k_y^2)\, \tilde{\psi}_{k_x,k_y} = 0. \tag{3.5}$$

This has solutions

$$\tilde{\psi}_{k_x,k_y} = C_{\pm} e^{\pm(z-h)\sqrt{k_x^2+k_y^2}-i(xk_x+yk_y)} \tag{3.6}$$

where C_+ and C_- are some constants (that depend on k_x and k_y). The solution with C_- increases with altitude, so it represents the magnetic field created by external currents. The other solution with C_+ gives the contribution from the internal currents.

The magnetic potential ψ can be determined by taking the horizontal Fourier-transform of the measured field, and fitting the coefficients $C_\pm$ for each wavenumber using Eqs. (3.3) and (3.6). It is evident that the horizontal part of the ground magnetic field can be fitted using either external or internal solution alone. Separation of the measured field into internal and external parts can be done by including the z-component in the analysis. This is discussed further e.g. by Chapman and Bartels (1940), Untiedt and Baumjohann (1993) and Pulkkinen et al. (2003b).

The equivalent currents themselves are calculated from the magnetic potential using the jump condition

$$\Delta \boldsymbol{B}_{\perp} = -\mu_0 \, \hat{\boldsymbol{e}}_z \times \boldsymbol{J}_{eq} \tag{3.7}$$

at some specific altitude, where the equivalent current sheet is assumed to be. For each individual plane wave, the ionospheric equivalent currents at $z = 0$ are given by

$$\tilde{\boldsymbol{J}}_{ion,eq} = \frac{-2iC_-}{\mu_0} \left(k_y \hat{\boldsymbol{e}}_x - k_x \hat{\boldsymbol{e}}_y\right) e^{h\sqrt{k_x^2+k_y^2} - i(xk_x + yk_y)}. \tag{3.8}$$

At small horizontal scales the factor $e^{h\sqrt{k_x^2+k_y^2}}$ becomes very large, and at these scales $\boldsymbol{J}_{ion,eq}$ can not be determined reliably. This happens because the magnetic disturbances created by small scale structures in the ionospheric currents decrease very rapidly with distance, so that the ground magnetic field is not affected by them. Also the sparseness of the ground magnetometer network may limit resolution at small wavelengths.

The Fourier-transform method described above is suitable for local studies, where the curvature of the Earth may be neglected. Similar analysis may be done using spherical harmonic functions in global scales (Chapman and Bartels, 1940) and spherical cap harmonic functions (Haines, 1985) in regional scales. One shortcoming of these spectral methods is that fixed upper and lower scale length must be chosen for the whole analysis area. Variations that are smaller or larger than these scale lengths cannot be modeled accurately. This is a problem if the spatial distribution of magnetometers is not uniform, as the minimum scale length must be chosen according to the sparsest region of the network.

The upward continuation method based on spherical elementary current systems (SECS), developed by Amm and Viljanen (1999) and further tested by Pulkkinen et al. (2003a), offers a flexible way of calculating the equivalent currents either in global or local scales. In this method the equivalent current is assembled from spherical elementary currents systems (SECS, see Appendix A for the related discussion). Several SECSs are placed at different locations on the ionospheric shell, and their magnitudes are chosen so that the best possible fit with measurements is obtained. The density of SECS may be different at different locations, so that areas with dense observations are processed with a better spatial resolution. In Paper I we introduced a new 1-dimensional variant of the elementary system method. This is discussed further in Section 3.1.3.

3.1.2 Relationship between real and equivalent ionospheric currents

An important question about the ionospheric equivalent currents is their relation to the real currents. In general, these two current systems may be quite different, so that a direct comparison is not possible. However, if we use the thin-sheet approximation, where also the real horizontal ionospheric currents are assumed to flow in a 2-dimensional sheet, some (approximate) relationships exist.

The true sheet current density $\boldsymbol{J}$ can be divided into divergence- and curl-free parts, so that

$$\boldsymbol{J} = \boldsymbol{J}_{CF} + \boldsymbol{J}_{DF}, \tag{3.9}$$

where

$$\nabla \cdot \boldsymbol{J}_{DF} = 0 \quad \text{and} \quad (\nabla \times \boldsymbol{J}_{CF})_z = 0. \tag{3.10}$$

If the background magnetic field is perpendicular to the ionospheric plane, then the true curl-free current system $\boldsymbol{J}_{CF}$ together with associated FAC does not produce any magnetic field below the ionosphere. Fukushima (1976) derived this result by assuming uniform ionospheric conductances, but the result is actually valid for any conductance distribution. According to Fukushima's theorem the ground magnetic disturbance is created by the divergence-free part of ionospheric sheet currents. As discussed in the previous Section, the ionospheric equivalent currents can be uniquely defined as divergence-free sheet currents that produce the observed magnetic field below the ionosphere. This means that for a vertical background magnetic field equivalent currents are the same as the divergence-free part of the true currents,

$$\boldsymbol{J}_{DF} = \boldsymbol{J}_{eq,ion}. \tag{3.11}$$

In particular, the curl of the horizontal currents can be calculated using the equivalent currents, as in Eq. (2.3).

The result in Eq. (3.11) is exactly valid only with a vertical background magnetic field. Away from the magnetic poles the inclination of the field lines means that also the divergent current system and associated FAC create some magnetic disturbances on the ground. The equivalent currents model also these disturbances, as illustrated in Fig. 3.1, so Eq. (3.11) is no longer valid. However, according to Untiedt and Baumjohann (1993) the effect of the tilted field lines is quite small for inclination angles $\chi \gtrsim 75^\circ$. This covers the auroral zone and also most of the MIRACLE network illustrated in Fig. 2.1.

Usually Eq. (3.11) is all we can say about the real ionospheric currents using just ground magnetic data. If we have some further information about ionospheric conductances, FAC or electric field, we may proceed with some of the analysis methods described in Section 2.2. In some special cases we may estimate the

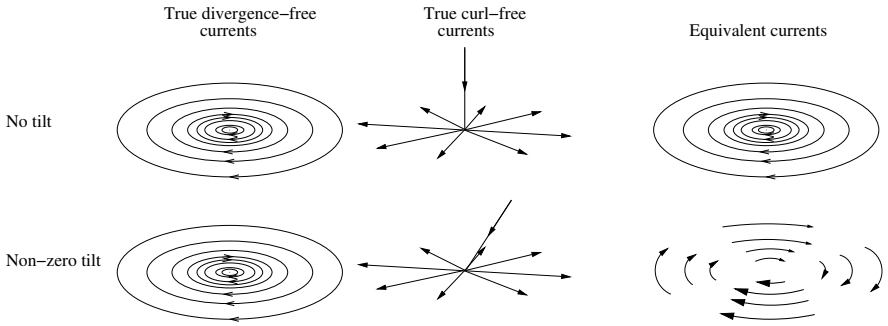

Figure 3.1: Schematic illustration of the effect of magnetic inclination on equivalent currents. **Upper part:** Background magnetic field is vertical and the true curl-free horizontal currents together with associated FAC are magnetically invisible below the ionosphere. Consequently, the equivalent currents are the same as the true divergence-free currents. **Lower part:** Background magnetic field has non-zero tilt and the curl-free current system creates some magnetic disturbances on the ground. Equivalent currents are no longer identical to the true divergence-free currents.

FAC directly from the equivalent currents. In some situations we may assume that conductivity gradients are parallel to the electric field, so that

$$\nabla\Sigma_P \times \boldsymbol{E} = 0 \quad \text{and} \quad \nabla\Sigma_H \times \boldsymbol{E} = 0.$$

If we further assume that the conductance ratio $\alpha = \Sigma_H/\Sigma_P$ is a constant, Eqs. (2.1)-(2.3) give us a relation between the equivalent currents and FAC,

$$j_\parallel = \frac{1}{\alpha}\left(\nabla \times \boldsymbol{J}_{eq}\right)_z . \tag{3.12}$$

This line of reasoning was applied by Amm et al. (2002) for a pair of traveling convection vortices, which exhibited a large degree of symmetry. However, these assumptions are usually too restrictive to apply. Conductivity gradients often have a component perpendicular to $\boldsymbol{E}$, and although the conductivity ratio α varies less than the conductances themselves, it is usually not a constant over large areas.

3.1.3 1-dimensional equivalent currents

The analysis methods mentioned in Section 3.1 can be used with data from a 2-dimensional ground magnetometer network, which extends at least a few hundred km both in latitude and longitude. However, in some cases we have data only

from a single line of magnetometers, which is usually oriented along the (magnetic) North-South direction. Examples of this kind 1-dimensional magnetometer lines are the coastal magnetometer chains in Greenland [11] and the 210 degree magnetometer chain [12]. The various methods discussed previously cannot be directly applied to data from a magnetometer chain, because there is not enough information to determine the 2-dimensional distribution of ionospheric equivalent currents.

In Paper I we present a modified, 1-dimensional version of the SECS method mentioned in Section 3.1. In the new 1D SECS method ionospheric equivalent currents are assumed to be azimuthally symmetric, so that the currents and ground magnetic field change only in the latitudinal direction. Of course, different 1-dimensional analysis methods have been developed also previously, e.g. 1D spherical harmonic analysis (Chapman and Bartels, 1940), 1D Fourier analysis (Mersmann et al., 1979) and line current method (Popov et al., 2001). However, all previous methods have some limitations in their use. The 1D spherical harmonic analysis requires global data coverage, whereas the 1D Fourier method neglects the curvature of the Earth. Additionally, in these spectral methods some minimum resolved wavelength must be chosen, as discussed in Section 3.1. This limits the flexibility of the methods, especially in situations where the magnetometer line has areas of very different spatial resolution. In the line current method the ionospheric equivalent currents are composed of individual (East-West directed) infinite line currents. This allows one to use different resolutions along the magnetometer line. In this method the curvature of the Earth is modeled correctly in the North-South direction (along the magnetometer line), but not in the East-West direction. Instead of bending around the Earth in the East-West direction, the line currents flow straight along the tangent line.

The new 1D SECS method was tested in several modeled 1-dimensional electrojet situations. The magnetic disturbances created by the model currents were calculated at selected IMAGE stations (see Fig. 1 of Paper I), and this simulated magnetic data was used in the 1D SECS method. It should be mentioned that 1D SECS were used also in the modeling step, in calculation of the ground magnetic disturbance. However, the spatial resolution in the modeling step was quite much finer than in the analysis step, so we probably did not commit an inverse crime[1], at least not very large one. The same model cases were analyzed using another technique, the 1D Fourier method (Mersmann et al., 1979). In addition to simulated electrojet events, we also studied several real cases. In these cases the previously introduced 2-dimensional SECS method (Amm and Viljanen, 1999; Pulkkinen et

[1] An inverse crime is committed when exactly the same procedure is used when preparing the model data (in this case the ground magnetic field $\boldsymbol{B}_G$), as is used when analyzing the data (in this case calculating $\boldsymbol{J}_{eq}$ from $\boldsymbol{B}_G$). This may lead to deceptively good results (e.g. Lionheart, 2004).

al., 2003a) was used as the "correct" reference solution. In the comparisons it became clear that the new 1D SECS method is much more accurate than the earlier 1D Fourier approach.

As a side note, in Paper I we also compared magnetic IU and IL indices[2] with integrated East-West currents flowing over the IMAGE magnetometer chain. The IU and IL indices should describe the strength of the eastward and westward electrojets over the IMAGE array, respectively. In Paper I we conclude that the indices give a reasonable estimate of the total currents flowing across the magnetometer chain, but not all features are estimated reliably. This is illustrated in Fig. 3.2. Partly the differences may be caused by the fact that the IU and IL indices measure the maximum instantaneous current density that is present at some latitude, but the total current is an integral over the latitude range covered by the magnetometer line. It should also be noted that we did not separate the internal and external parts of the ground magnetic field in the analysis (it is not separated in the indices either). The internal part of the magnetic field will lead to an overestimation of the ionospheric currents by a few tens of percents, as was shown by Tanskanen et al. (2001). However, accurate separation of the internal and external fields would require a very dense magnetometer network (densest part of IMAGE in Fig. 2.1 is about the lower limit, Pulkkinen et al., 2003b), so it is rarely done in practice. The main advantage of the indices is their easy calculation. However, also the 1D SECS method is quite easy to use and computationally efficient, so that the latitudinal profiles of equivalent currents can be constructed almost as easily as the IU and IL indices.

The 1D SECS method introduced in Paper I was developed for ground magnetic studies. Recently Juusola et al. (2006) have generalized the method and applied it to satellite measurements. Measurements along a single satellite track form naturally a 1-dimensional chain. Above the ionosphere also the curl-free current system produces magnetic disturbances, so that the whole current system can be determined. In the 1D SECS method both satellite and ground based magnetic measurements can be used simultaneously in the analysis, so that the best possible agreement with observations is obtained.

3.2 Traditional KRM method and a new approach

The KRM method developed by Kamide et al. (1981) was briefly discussed in Section 2.2. A more thorough introduction to the KRM method is given in Paper II, where we also present a new approach to solving the same problem.

The problem of obtaining the ionospheric electric field using ground magnetic

[2]Local variants of the AU and AL indices. See Kauristie et al. (1996).

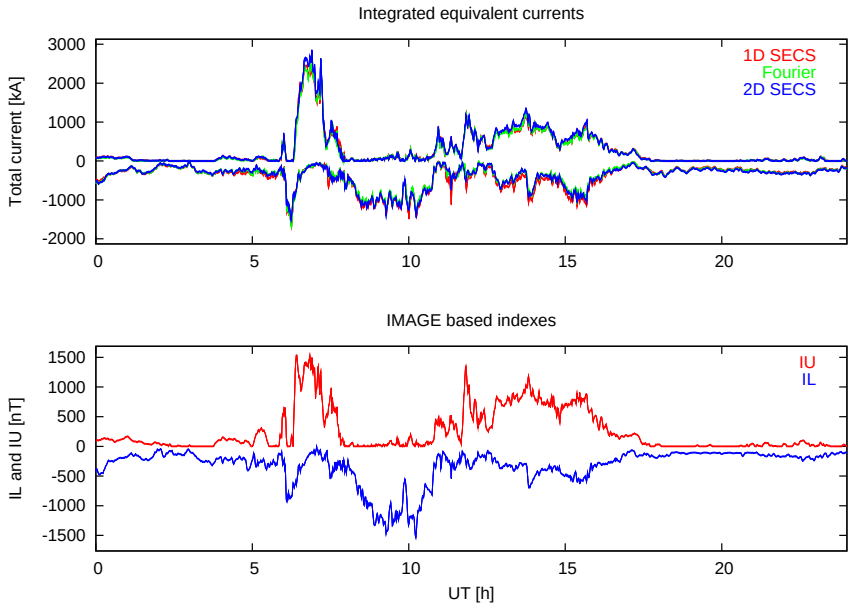

Figure 3.2: Same as Fig. 12 of Paper I. Integrated eastward (+) and westward (-) currents for 24/11/2001, together with IMAGE based indices IU and IL. Integrated currents are calculated using 3 different methods: 1- and 2-dimensional elementary currents (1D and 2D SECS) and 1-dimensional Fourier method. See Paper I for further details.

measurements (or equivalent currents) and estimated ionospheric conductances as input data was extensively studied in the 1970's and early 80's (see e.g. Kamide et al., 1981; Murison et al., 1985; Untiedt and Baumjohann, 1993, and references therein). The standard solution technique, known as the KRM method, was developed by Kamide et al. (1981). The basic idea is to find such a potential electric field that together with Ohm's law it is consistent with the equivalent currents obtained from magnetic measurements. The details are discussed further in Paper II.

The KRM method works well in global scales (Wolf and Kamide, 1983), but in regional studies the unknown boundary conditions for the electric potential at the borders of the analysis area are problematic. This was demonstrated by Murison et al. (1985), who studied a Harang discontinuity situation using data from northern Scandinavia. Murison et al. (1985) solved the problem using the KRM method and several different boundary conditions. Their results show that the solution, i.e. the electric field, total ionospheric currents and FAC, depends

quite strongly on the boundary conditions imposed on the electric conductance. Without any a priori information about the electric field, the correct boundary conditions cannot be determined. This limits the applicability of the KRM method in regional studies, where the analysis area is typically only a few hundred or a few thousand km across.

Our goal in Paper II is to develop a better alternative to the traditional KRM method, especially in regional studies. We use the same set of input data as in the KRM method, but our mathematical approach is significantly different. As explained in Section 3.1.2, the divergence-free part of the ionospheric currents can be determined from ground magnetic measurements, but the curl-free part is magnetically invisible below the ionosphere. Our approach is to find such a curl-free part of the current, that the total current system, together with Ohm's law, is consistent with a potential electric field. The traditional KRM approach and the new formulation are closely related. If one approach is valid, so is the other one too. However, the resulting differential equations (Eqs. (4) and (8) in Paper II) are somewhat different. The largest difference is that in the KRM method only $(\nabla \times \boldsymbol{J}_{eq})_z$ enters the equation, whereas in the new approach the whole vector $\boldsymbol{J}_{eq}$ is needed. As mentioned in Paper II, in a limited area $\boldsymbol{J}_{eq}$ may have a Laplacian part that has zero curl inside the analysis area (divergence is zero by definition). This part of $\boldsymbol{J}_{eq}$ does not contribute to the KRM solution, but is included in the new approach.

In Paper II we also develop a new numerical method for solving our differential equation. This method is based on the Cartesian elementary current systems (CECS) basis functions. The properties and use of CECS are reviewed in Appendix A. With the elementary systems any 2-dimensional vector field can be presented in terms of its curl and divergence. The numerical CECS-based solution method described in Paper II is essentially a kind of finite element method (FEM) for the sources of the electric field and current system. The differential equation for the current potential is converted into a system of linear algebraic equations, which can be solved using standard matrix techniques. In summary, the calculation algorithm based on the elementary systems is the following:

- Calculate the electric field $\boldsymbol{E}_1$ that is consistent with Ohm's law and the conductances and equivalent currents given as input data.
- Divide $\boldsymbol{E}_1$ into curl- and divergence-free parts.
- Construct a relation between the unknown curl-free part of the current $\boldsymbol{J}_{CF}$ and the electric field $\boldsymbol{E}_2$ consistent with it.
- Solve for $\boldsymbol{J}_{CF}$ using the condition that the total electric field $\boldsymbol{E}_1 + \boldsymbol{E}_2$ is curl-free.

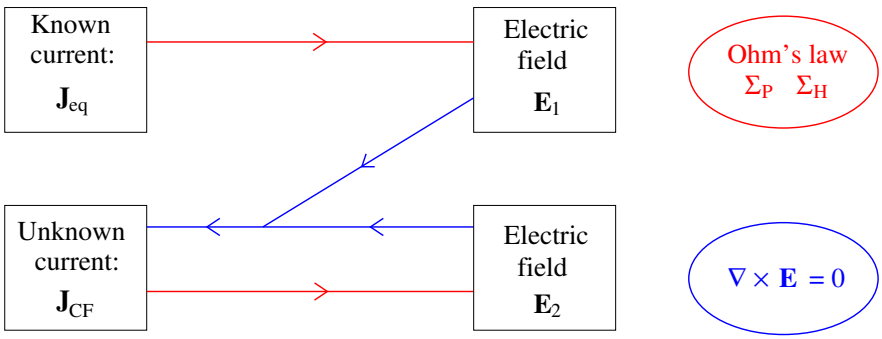

Figure 3.3: Flow chart of the CECS-based solution technique. See text and Paper II for further details.

This calculation procedure is represented as a flow chart in Fig. 3.3. Perhaps the main advantage of the CECS method is the inclusion of boundary conditions. With CECS the vector fields are constructed from divergences and curls, so the natural and automatically included boundary condition is to assume that outside the analysis area the vector fields are divergence- and curl-free. This is probably not the correct boundary condition in all situations, but it is very natural and convenient.

The CECS-based numerical technique could be used also with the original KRM formulation. In that case we would expand the electric field in terms of curl-free CECS and solve them using Ohm's law and the condition that the curl of the current has to be the same as the curl of the equivalent currents. However, the new approach for solving the currents instead of the electric field makes a better use of the information contained in the equivalent current vector $\boldsymbol{J}_{eq}$. This is especially important in the local scale studies, as discussed above.

The new features of our calculation method should make it ideal for local scale studies, where the traditional KRM method is prone to errors. This is verified in Paper II, where we compare the KRM method and our new approach in several realistic model situations. In all studied cases the new calculation method gives much more reliable estimates of the ionospheric electric field and current system. Of course, if correct boundary conditions could be determined, the KRM method would give similar results.

Recently, Kamide et al. (2003), Shirai et al. (2003) and Ieda and Kamide (2005) have described a way of using the KRM method in near real-time for regional ionospheric monitoring. The idea is to use the AMIE procedure (see Section 2.2) for obtaining a rough estimate of the global electric field structure, and then refine the result by using the KRM method in regions of good data cover-

age. In this approach the boundary conditions for the KRM solution are obtained from the AMIE results. However, it should be noted that in absence of global data coverage AMIE will give results that are mostly based on statistical models. This means that the boundary conditions, and hence the KRM solution, may not be accurate enough for studying specific events in detail.

The calculation method presented in Paper II was developed especially for local studies. However, as mentioned in the paper, it can be used also in global scales. The only limitation is the assumption of a vertical background magnetic field, which is not a valid approximation with inclination angles $\chi < 75^\circ$ (Untiedt and Baumjohann, 1993).

3.2.1 Effect of different conductance distributions on the KRM solution

As discussed in Paper II, the ionospheric Hall and Pedersen conductance distributions used as input data may be quite difficult to obtain in practice. We also list several possible sources of conductance estimates:

- Satellite images of auroral UV- and X-ray emissions (Lummerzheim et al., 1991)
- All-sky camera images (Partamies et al., 2004; Robinson et al., 1987)
- Statistical models, like Fuller-Rowell and Evans (1987) or [4]
- Correlation with ground magnetic field (Ahn et al., 1983;1998).

All these methods have some shortcomings. Statistical models or estimates based on ground magnetic disturbances are not very accurate, especially during disturbed conditions. Satellite or all-sky camera images do not always have a sufficient spatial and/or temporal coverage. In addition, several model parameters or empirical relations must be assumed, before ionospheric conductances can be estimated from the images. In practice, reliable conductance estimates based on all-sky camera images are hard to obtain.

In addition to the above mentioned methods, ionospheric conductances can also be estimated using incoherent scatter radars (e.g. Lühr et al., 1998) or particle precipitation data from satellites (e.g. Vondrak and Robinson, 1985). However, these methods give only pointwise estimates, not 2-dimensional conductance distributions. For a further discussion on conductance estimates and for a comparison between ground and satellite based estimates, see Aksnes et al. (2005).

The dependence of the KRM solution on different conductivity distributions has been studied by Kamide and Richmond (1982) and Murison et al. (1985).

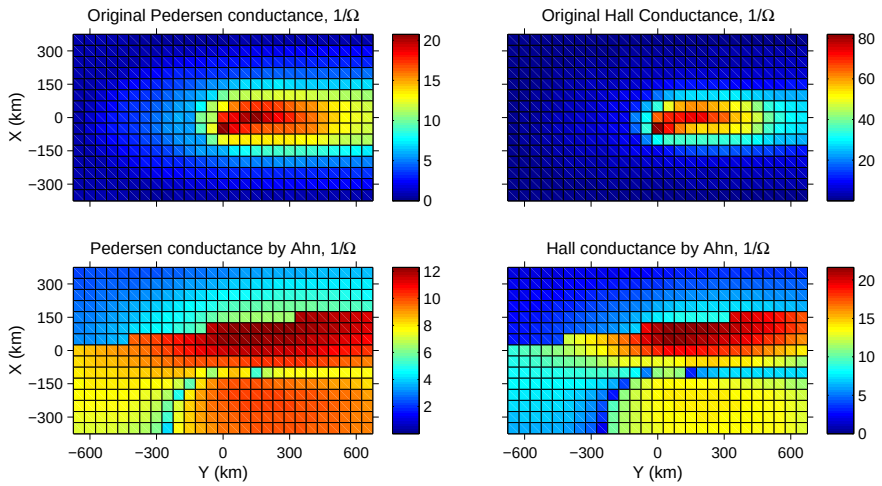

Figure 3.4: The "correct" conductance distribution in the WTS model by Amm (1996) (top row) and the conductance distribution obtained using model by Ahn et al. (1998) (bottom row).

Kamide and Richmond (1982) conclude that the horizontal ionospheric currents are quite insensitive to the input conductivity distribution, while the electric field depends strongly on the conductances. This is explained by the fact that the input equivalent currents form the usually dominant divergence-free part of the total ionospheric currents, as discussed in Section 3.1.2. Equivalent currents are determined directly from the ground magnetic field, so they do not depend on the conductances. Kamide and Richmond (1982) found that the FAC, and hence horizontal curl-free currents, are affected by the choice of the conductance model, but not as strongly as the electric field. This can be expected from consideration of a uniformly conducting ionosphere (Kamide et al., 1981). In that case (assuming $\nabla \times \boldsymbol{E} = 0$) the electric field would be inversely proportional to the Hall conductance,

$$\nabla \cdot \boldsymbol{E} = (\nabla \times \boldsymbol{J}_{eq})_z / \Sigma_H. \tag{3.13}$$

On the other hand, FAC would depend just on the conductance ratio, as in Eq. (3.12). Thus it seems that the KRM method should give more reliable estimates of the FAC, and especially of the total horizontal currents, whereas the electric field estimates depend strongly on the input conductances. A similar behavior is expected for the new CECS-based calculation method as will be demonstrated below.

Figure 3.4 shows the original conductance distribution of the WTS model, used in Paper II, together with the conductance estimate obtained from the ground magnetic disturbance using the method by Ahn et al. (1998). Although the model

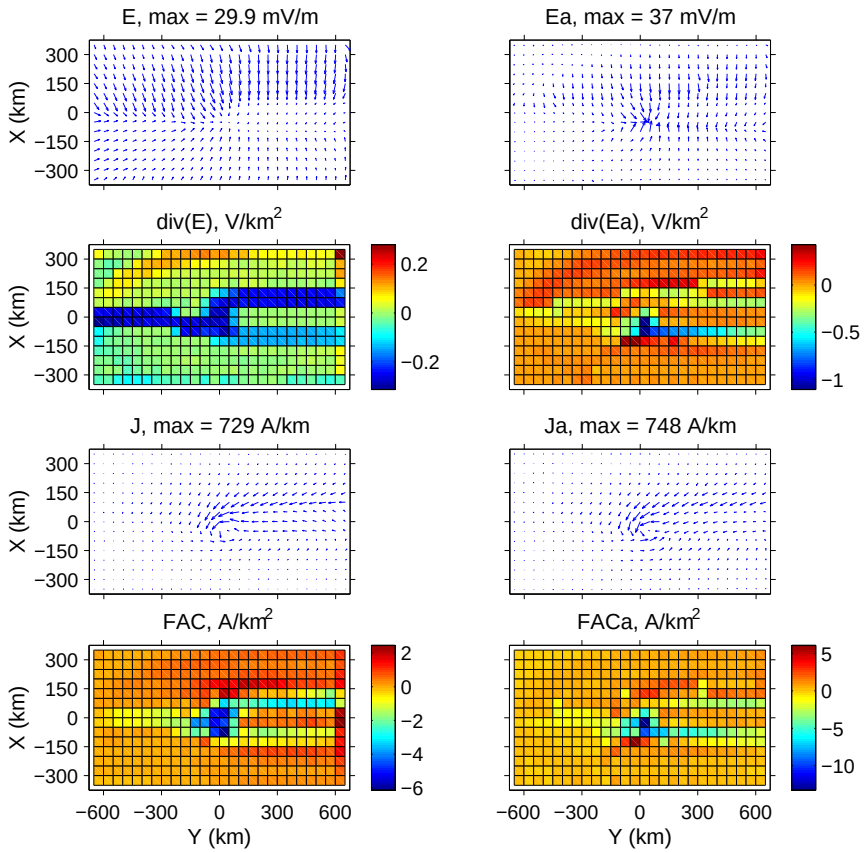

Figure 3.5: The CECS method results for the WTS case using the "correct" conductance distribution (left column, same as in Fig. 10 of Paper II) and using the conductance estimate by Ahn et al. (1998) (right column).

by Ahn et al. (1998) may give quite reasonable estimates of the large scale conductance distribution on the average, in this particular case the agreement with the data-based model is quite poor. The sharp conductance gradients in the estimate are caused by the different coefficient used by Ahn et al. (1998) for the poleward and equatorward sides of the eastward and westward electrojet regions.

The two different conductance distributions shown in Fig. 3.4 are used as input data in the new CECS-based calculation technique. The results of the calculations are shown in Fig. 3.5. The results obtained using Ahn's conductivity estimate are quite different from the results obtained with the correct conductances. With the correct input conductances the CECS-method is able to reproduce the model system with a good accuracy, as demonstrated in Paper II. However, when the Ahn

estimate is used, the resulting electric field is very different. The underestimated conductances near the center of the WTS system result in a grossly overestimated electric field. Nevertheless, there are still some structural similarities between the two solutions, e.g. the divergence of electric field at the center and the change from southward to northward electric field. The FAC are not affected as much by the choice of the conductance model. With Ahn's conductance model the magnitude of the FAC is overestimated due to the too low conductances, but the shape of the spatial distribution is in a qualitative agreement with the other solution. The total horizontal current system is dominated by the equivalent currents, so it is not really affected by the choice of the conductivity model. These results are in agreement with those obtained by Kamide and Richmond (1982), and demonstrate the importance of reliable conductance estimates in applications of the KRM or new CECS methods.

Chapter 4

Role of inductive phenomena in ionospheric electrodynamics

In this Chapter we discuss the role of inductive phenomena in ionospheric electrodynamics and in the ionosphere - solid earth connection. Traditionally it has been assumed that inductive phenomena in the ionosphere are negligible. This is a central assumption in many of the analysis methods reviewed in Section 2.2, because it allows us to present the ionospheric electric field in terms of a potential, as in Eq. 1.5. However, in certain very dynamical situations this assumption is not valid, and the electric field has also a considerable induced rotational part. Analysis of such situations and development of suitable calculation techniques is undertaken in Papers III-V, and forms a central part of this Thesis.

First in Section 4.1 we describe the reflection of Alfvén waves at the ionospheric boundary and the role of ionospheric induction in the reflection process. The induction studies performed in Papers III-V are discussed in Section 4.2. Finally in Section 4.2 we briefly discuss the inductive coupling between the ionosphere and the solid earth.

4.1 Reflection of Alfvén waves at the ionosphere

Ionospheric and magnetospheric plasmas support a large number of different wave modes (e.g., Parks, 1991; Baumjohann and Treumann, 1997), among them the Alfvén waves (or magnetohydrodynamic waves). There are three different types of Alfvén waves: Shear mode and fast and slow magnetosonic modes[1]. The fast mode wave is able to propagate in all directions with respect to the background magnetic field, but the shear mode propagates along the background magnetic

[1]Shear mode is also called transversal or torsional mode or simply the Alfvén wave. Fast magnetosonic wave is also called compressional wave

field. This way the shear Alfvén waves transport energy, momentum and angular momentum efficiently between different regions in the magnetosphere-ionosphere system (Vogt, 2002). If some disturbance, like a solar wind pressure pulse, creates MHD waves in the magnetosphere, a part of the shear mode waves are guided by the magnetic field to the Earth's polar ionospheres. Typical wavelengths of the magnetospheric Alfvén waves are much larger than the thickness of the ionospheric current layer. Therefore the incident waves see the ionosphere as a thin, well conducting sheet, and may be reflected at this boundary.

A simplified model of the reflection of Alfvén waves from the ionosphere is following:

- Ionosphere is a thin horizontal sheet with uniform Pedersen and Hall conductances.
- Above the ionosphere there is perfectly conducting and collisionless plasma that supports the Alfvén wave modes.
- No currents flow in the neutral atmosphere below the ionosphere.
- The background magnetic field is assumed to be perpendicular to the ionospheric plane.

We can further assume that the incident wave is in the shear mode, because fast magnetosonic waves are not guided by the geomagnetic field and therefore they experience geometric attenuation. The classical reflection coefficient by Scholer (1970) can be derived from current continuity in the ionospheric boundary. The electric fields of the incident and reflected shear waves at the ionospheric boundary are denoted as $\boldsymbol{E}^{\downarrow}$ and $\boldsymbol{E}^{\uparrow}$, respectively. These wave fields are perpendicular to the background magnetic field and also irrotational (Vogt, 2002),

$$(\nabla \times \boldsymbol{E}^{\downarrow})_z = 0, \qquad (\nabla \times \boldsymbol{E}^{\uparrow})_z = 0.$$

The total ionospheric electric field is just the sum of the wave fields,

$$\boldsymbol{E} = \boldsymbol{E}^{\downarrow} + \boldsymbol{E}^{\uparrow}. \tag{4.1}$$

The shear waves carry a FAC given by (Vogt, 2002)

$$j_{\parallel} = \Sigma_A \nabla \cdot (\boldsymbol{E}^{\downarrow} - \boldsymbol{E}^{\uparrow}), \tag{4.2}$$

where $\Sigma_A = 1/(\mu_0 v_A)$ is the Alfvén conductance and v_A the Alfvén speed of the waves. The FAC carried by the incident and reflected waves must be equal to

the FAC given by Ohm's law, Eq. (2.2). This condition, with the assumption of uniform conductances, gives the reflection coefficient for the shear waves,

$$\boldsymbol{E}^{\uparrow} = \frac{\Sigma_A - \Sigma_P}{\Sigma_A + \Sigma_P} \boldsymbol{E}^{\downarrow}. \tag{4.3}$$

This argument can also be generalized for non-uniform ionospheric conductances, in which case a differential equation for the electric potential of the reflected wave is obtained (Glassmeier, 1984).

Alfvén wave propagation and reflection at the ionosphere is associated with pulsations in the ground magnetic field. Field line resonances (Kivelson and Southwood, 1985, 1986), ionospheric waveguide (Greifinger and Greifinger, 1968) and ionospheric Alfvén resonator (Polyakov and Rapoport, 1981) are all examples of Alfvén wave activity related to magnetic pulsations. See e.g. Yoshikawa et al. (1999), Lysak (2004) and Streltsov and Lotko (2004) for further discussion and details on recent modeling results. Reflection of Alfvén waves at the ionosphere also enables a feedback mechanism between the ionosphere and magnetospheric regions driving the auroral current system (e.g. Vogt, 2002).

4.1.1 Inductive effects in the Alfvén wave reflection

In the above calculation inductive effects in the ionosphere were not included, and we explicitly assumed the ionospheric electric field to be given as a sum of irrotational shear waves. However, changing magnetic fields in the ionosphere create an inductive rotational electric field, which in turn is associated with a fast mode wave. This effect is an important factor in the ionospheric waveguide (Greifinger and Greifinger, 1968), where fast mode waves are trapped around the F-layer density maximum. Also some other authors (e.g. Hughes and Southwood, 1976; Glassmeier, 1984) considered the role of inductive electric fields in the ionosphere. However, the consequences of the inductive fields were considered negligible for typical ionospheric conditions, and inductive effects were largely ignored, either implicitly or explicitly. More recently, Yoshikawa and Itonaga (1996) and Buchert (1998) showed that inductive effects may have a large impact on the reflection of Alfvén waves. When ionospheric self-induction is included, the incident shear wave is reflected as both shear and fast mode waves. The induced rotational electric field associated with the fast mode wave drives additional FAC, and consequently modifies the ionosphere-magnetosphere coupling. The simple reflection coefficient of Eq. (4.3) has to be replaced with a reflection tensor, which depends on the frequency and horizontal wavelength of the incident wave, as well as on ionospheric Hall and Pedersen conductances. The reflection coefficients R_A (shear wave→shear wave) and $R_{A\to F}$ (shear wave→fast wave) obtained by Yoshikawa and Itonaga (1996) are illustrated later in Section 4.3.

Yoshikawa and Itonaga (1996) and Buchert (1998) were able to obtain analytical results for a simple case with uniform ionospheric conductances and a vertical background magnetic field. These results have later been applied and extended e.g. by Buchert and Budnik (1997) for an impulsive magnetosphere-ionosphere coupling event, by Yoshikawa et al. (1999) for eigenmodes of field line oscillations and by Yoshikawa et al. (2002) for inductive shielding of geomagnetic pulsations. Sciffer et al. (2004) broadened the applicability of the method to lower magnetic latitudes by including oblique magnetic fields in the analysis.

According to the results by Yoshikawa (2002), neglect of the inductive response of the ionosphere is a valid approximation if the condition

$$\frac{\omega \mu_0 \Sigma_P}{k_\perp (1 + \coth k_\perp d)} << 1 \tag{4.4}$$

is satisfied (see also Lotko, 2004). Here ω is a typical angular frequency and $k_\perp$ a typical horizontal wavenumber of the ionospheric current system, and $d \approx$100 km is the height of the E-layer above the (presumed) perfectly conducting ground. It is evident that in the reflection of Alfvén waves inductive effects become more significant at large horizontal scales.

Lysak (1997) used quite a different approach to investigate the propagation of Alfvén waves in the magnetosphere-ionosphere system. The numerical model presented by Lysak (1997) and later refined by Lysak (1999, 2004) and Lysak and Song (2001) includes induction effects and (at least in principle) is able to use three-dimensional, height-resolved ionospheric conductivity distributions. These numerical calculations have verified the modifications to the reflection coefficients that were obtained by Yoshikawa and Itonaga (1996), as well as the mode coupling between shear and compressional waves and the horizontal propagation of the fast mode waves in the ionospheric wave guide, as proposed by Greifinger and Greifinger (1968).

4.2 New approach for modeling ionospheric induction

In Papers III-V we consider the inductive effects in the ionosphere in relation to some typical, specific ionospheric events. While the Alfvén wave models discussed in the previous Section have given us a better understanding of the ionospheric inductive phenomena and coupling of the ionosphere and magnetosphere, they are not really suitable for event studies. The main problem is that in all these models the spatial and temporal distribution of the incident Alfvén waves above the ionosphere is assumed to be known. This is quite a restrictive assumption in

practical studies, because the incident wave pattern is very hard to measure. To the author's knowledge there seems to be no empirical models of Alfvén wave patterns related to some specific ionospheric events. In principle one could use a magnetospheric MHD simulation as an input in the Alfvén wave scheme, but current simulations use electrostatic ionospheric solvers and it would not be straightforward to couple them to an ionospheric Alfvén wave solver (Janhunen, 1998). In addition, magnetospheric MHD simulations also have problems in reproducing specific ionospheric phenomena.

In Paper III we started to develop a different approach for solving the ionospheric induction problem. Our goal is to use only ionospheric parameters as input, so that specific events can be easily studied. In Paper III we use a very simple approach, where the ionospheric potential electric field and associated current system are assumed to be known as a function of time and position. The induced electric field due to ionospheric self induction is calculated simply by taking the time derivative of the vector potential created by the input currents. The induced field is then compared to the original potential field, so that the relative contribution by induction can be estimated. In Paper III we also considered the inductive coupling between the ionosphere and solid earth, which forced us to perform the calculations in the frequency domain. The ionospheric self-induction could have been calculated as well in the time domain. The results of the ionosphere - solid earth induction loop are discussed separately in Section 4.3.

It may seem bit controversial to assume that only the potential part of the ionospheric electric field is given as input parameter, while the induced part is calculated. If we use direct measurements or even empirical models as input, shouldn't we know the total electric field, potential + induced, from the beginning? As explained in Section 2.2, in many data analysis methods it is assumed that the electric field is given by a potential, so these methods give only potential fields as output. Also some more direct methods, like the SuperDARN mapping technique (Ruohoniemi and Baker, 1998), use the potential assumption. Direct measurements of rotational ionospheric electric fields are difficult, due to their spatial localization and often small amplitude. Rotational part of the electric field easily falls below the spatial resolution or noise level of radar measurements. For example, Lühr et al. (1998) speculated that there may be an inductive electric field of a few mV/m in the WTS system, but they were not able to confirm this, as they used only single point measurements from the EISCAT incoherent scatter radar. At present, the best way of estimating the role of inductive phenomena in ionospheric electrodynamics is to assume some realistic model situation and calculate from first principles the induced rotational field that should be present in this situation. Of course, at some point we should be able to verify these estimates experimentally.

It should be emphasized that the results of Paper III are quite approximative.

Simply taking the time derivative of the vector potential created by some input current system is correct in vacuum, but not in the conductive ionosphere. The induced electric field itself drives some extra currents, and the effects of these currents are not included in the analysis of Paper III. Additionally, the induced electric fields calculated in Paper III are not totally divergence-free. This is because the induced field created by changing curl-free currents (Eq. 9 in Paper III) has a potential-like horizontal component. The total 3-dimensional induced electric field is purely rotational, but the horizontal part at the ionospheric plane is not. This was not considered further in Paper III, but in retrospect the electric field induced by changing curl-free currents should not be included in the analysis. The potential-like induced horizontal field would quickly be canceled by charge accumulation in the conducting ionosphere. Despite these shortcomings of the simple calculation, we believe that the results obtained in Paper III are good order of magnitude estimates, and give a realistic picture of the role of induction in ionospheric phenomena.

In Paper III we calculated the induced electric field for several different ionospheric phenomena using realistic, data-based models. These included the WTS and Ω-band models described in Section 2.3.3. We found that the induced electric fields and associated currents were not negligible in the most dynamical situations, like the WTS. The maximum strengths of the induced electric fields were relatively low, just a few mV/m, but the fields were concentrated in local "hot spots" at areas of enhanced ionospheric conductance. At these locations also the potential electric fields were suppressed and comparable to the induced fields. At the areas of enhanced conductances even the relatively weak induced electric fields generate large horizontal and field aligned currents, so in Paper III we concluded that inductive effects may have large impact on ionospheric phenomena and also ionosphere-magnetosphere coupling.

On the basis of the preliminary results in Paper III, we started to develop a self-consistent way of calculating ionospheric induced electric fields. This new method is presented in Paper IV and applied to some specific model events in Paper V. The calculation technique is based on dividing the electric field and ionospheric currents into divergence- and curl-free parts, which is easily done using CECS (see Paper IV and Appendix A). Ohm's law, Ampere's law and Faraday's law are used to construct a system of linear algebraic equations between the given potential electric field and the unknown rotational electric field. The flow chart in Fig. 4.1 illustrates the calculation process. The resulting matrix equation can be easily solved using standard inversion techniques. It should be emphasized that also in the new calculation method only ionospheric conductances and potential electric field are used as input parameters. This makes the new method easily applicable to specific ionospheric events.

The event studies in Paper V confirm the earlier, more approximate results

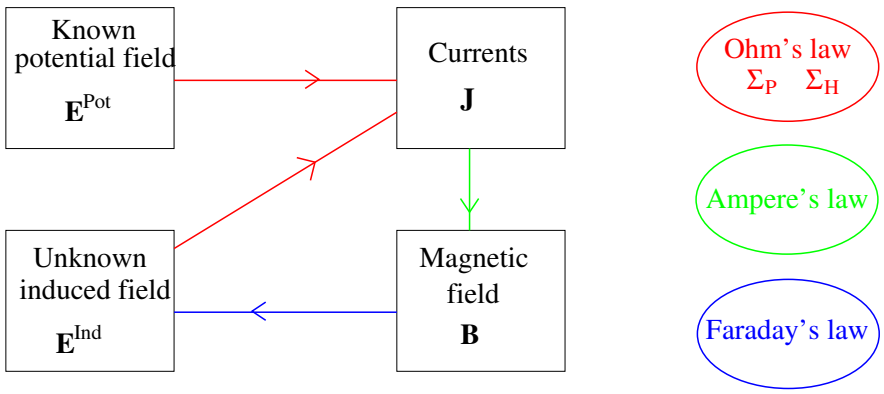

Figure 4.1: Flow chart of the calculation method developed in Paper IV. Ionospheric potential electric $\boldsymbol{E}^{Pot}$ and conductances Σ_P, Σ_H are given as input, while the induced rotational part of the electric field $\boldsymbol{E}^{Ind}$ is unknown. Ohm's law connects the electric fields and currents, Ampere's law connects the currents and magnetic field and Faraday's law connects the magnetic field and induced electric field. See Papers IV and V for further details and examples.

obtained in Paper III about the magnitude of the inductive electric fields and currents. There are also some differences in the results of the two calculation methods. The differences are caused by the approximations done in Paper III, where the induced electric field was calculated as in vacuum and it was not completely divergence-free. These aspects are handled correctly in Papers IV and V. In the WTS, Ω-band and electrojet events studied in Paper V, the induced electric field has typical values of a few mV/m. This amounts to several tens of percents of the potential electric field present at the same locations. The induced electric field is associated with ionospheric and field aligned currents that modify the overall structure of the current systems. Especially the induced FAC are often comparable to the non-inductive FAC, and may thus modify the coupling between the ionosphere and magnetosphere in dynamical events. This is illustrated in Fig. 4.2 where the ratios between induced and total electric fields and FAC in the WTS system are shown. The inductive electric field and FAC are limited to a relatively small "hot-spots" around the surge center, but there they have a significant impact on the electrodynamics.

Lenz's law states that the direction of the induced electric field in a loop of wire is such that the induced current opposes the change of magnetic flux through the loop. At first one might think that according to Lenz's law the induced ionospheric currents should oppose the original currents. However, this is not the case, as can be seen in the examples presented in Paper V. In many cases induction

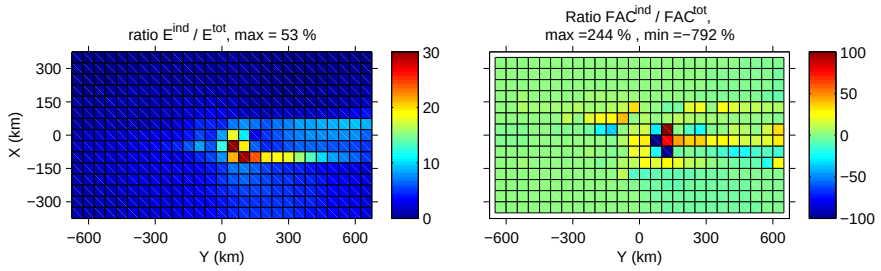

Figure 4.2: The ratios between the induced and total electric field and FAC in the westward traveling surge (WTS) model. Reproduced from Fig. 8 of Paper V.

seems to enhance the change in FAC flowing between the ionosphere and magnetosphere. This somewhat counterintuitive result is explained in Fig. 4.3, which is a schematic presentation of Lenz's law in ionospheric electrodynamics. It should be noted that only rotational currents are associated with the z-component of magnetic field that goes through the ionospheric plane (see Eqs. (A.10) and (A.11) in Appendix A). The induced currents oppose the change in the rotational current, and hence also the change of magnetic flux through the ionospheric plane, but enhance the change in the divergent currents. This tendency of inductive currents to enhance the change of FAC was also noted by Buchert (1998) and Yoshikawa and Itonaga (2000).

As a further note we present an easy way to estimate the importance of induction in a specific event. In Paper V we made some simple estimates of the induced electric field using the time-derivative of the equivalent currents (Eq. 2 and Fig. 10 in Paper V). Here we make a more basic derivation. The electric field is divided into two parts,

$$\boldsymbol{E} = \boldsymbol{E}^{pot} + \boldsymbol{E}^{ind}, \tag{4.5}$$

where $\boldsymbol{E}^{pot}$ is the potential part and $\boldsymbol{E}^{ind}$ the induced rotational part. We can approximate the z-component of Faraday's law as

$$|\boldsymbol{E}^{ind}| \approx B_z L/T, \tag{4.6}$$

where T is a typical time scale and L a typical length scale. The z-component of the magnetic field is related to the divergence-free currents (see Eqs. (A.10) and (A.11) in Appendix A). From Ampere's and Ohm's laws we get

$$\Delta \boldsymbol{B}_{\perp,DF} = \mu_0 \boldsymbol{J}_{DF} \approx \mu_0 \Sigma_P \boldsymbol{E}^{ind} + \mu_0 \Sigma_H \hat{\boldsymbol{e}}_z \times \boldsymbol{E}^{pot} \tag{4.7}$$

Here $\Delta \boldsymbol{B}_{\perp,DF}$ is the jump in horizontal magnetic field caused by the horizontal divergence-free sheet current $\boldsymbol{J}_{DF}$. In the last step we have assumed uniform

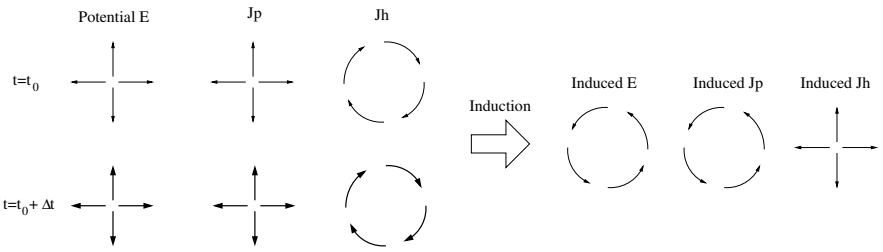

Figure 4.3: Lenz's law in ionospheric electrodynamics (assuming uniform conductances and downward pointing background magnetic field). Changes in the potential electric field ($\boldsymbol{E}^{pot}$) and associated currents ($\boldsymbol{J}_P$ and $\boldsymbol{J}_H$) create rotational induced electric field ($\boldsymbol{E}^{ind}$). Direction of $\boldsymbol{E}^{ind}$ is such that induced Pedersen currents oppose the *change* in rotational currents. This means that the induced Hall currents enhance the *change* in divergent currents and associated FAC. In the case of non-uniform ionospheric conductances the situation is more complicated (see text for further discussion). Same as Fig. 1 of Paper V.

ionospheric conductances. From Eq. (A.10) we see that

$$B_z = \Delta \boldsymbol{B}_{\perp,DF}/2 \tag{4.8}$$

Finally, from the above equations we can solve

$$|\boldsymbol{E}^{ind}| \approx \frac{\mu_0 \Sigma_H L/T}{2 + \mu_0 \Sigma_P L/T} |\boldsymbol{E}^{pot}| \tag{4.9}$$

We see that with very fast temporal changes and/or large spatial scales the limiting value is $|\boldsymbol{E}^{ind}|/|\boldsymbol{E}^{pot}| = \Sigma_H/\Sigma_P$. This is the same limit that is obtained with very high ionospheric conductances. At this limit the rotational currents driven by the potential and induced rotational fields cancel each other, so that the z-component of magnetic field through the ionospheric plane does not change.

The above estimate is compared against exact calculations in Fig. 4.4. The WTS is moving with different speeds V, and the induced field is estimated using values $\Sigma_P = 20$ S, $\Sigma_H = 60$ S, $|\boldsymbol{E}^{pot}| = 7$ mV/m and $L/T = V$ in Eq. (4.9), which are representative of the "head" of the WTS (see Fig. 8 in Paper V). Figure 4.4 shows that Eq. (4.9) gives quite good estimates for the magnitude of the induced field. Of course, the values Σ_P, Σ_H, $|\boldsymbol{E}^{pot}|$, L and T are somewhat subjective, and a different choice would give a different result. Equation (4.9) is also based on the assumption of uniform conductances, which is certainly not true in the WTS. In any case, we may conclude that the functional dependence on the conductances as well as on length and time scales seems to be correct in Eq. (4.9).

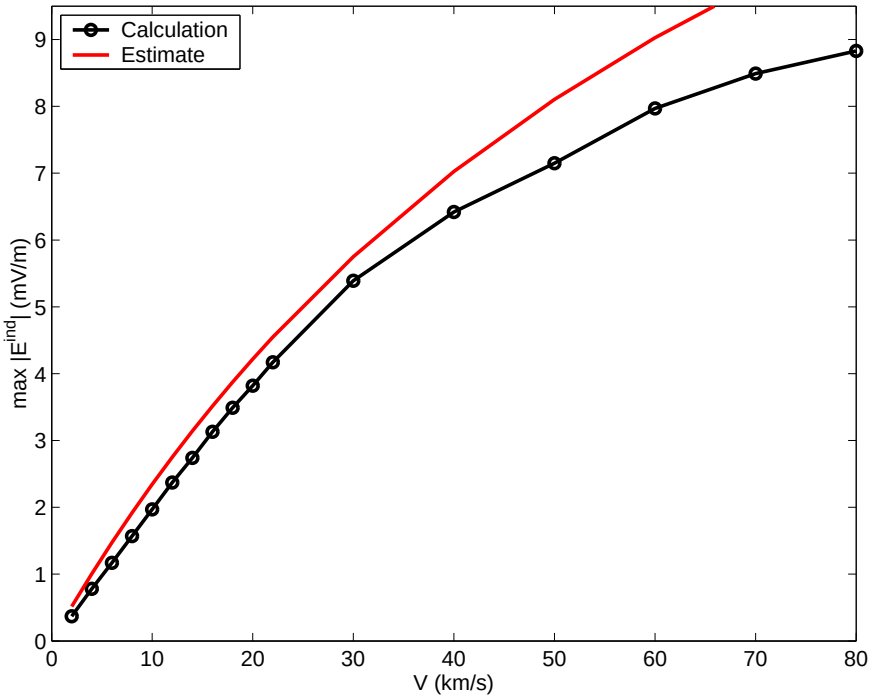

Figure 4.4: The magnitude of the induced electric field in the WTS as a function of the surge velocity. Calculations are from Fig. 12 of Paper V and the estimate is done using Eq. (4.9). Note that speeds V>10 km/s are unrealistic for the WTS, but they are used here to illustrate the non-linear nature of induction. See text for further details.

These dependences are also consistent with the scaling properties found in Paper V by numerical calculations.

4.3 Inductive coupling between the ionosphere and solid earth

As mentioned above, in Paper III we studied also the inductive coupling between the ionosphere and conducting ground. As discussed in Section 3.1, variations in external (ionospheric) currents and associated magnetic fields create induced electric fields in the ground. The ground is a relatively good conductor (resistivity of crust is typically 10-10000 Ωm, Korja et al., 2002), so the induced electric field drives large currents, which produce their own time-varying magnetic fields. The

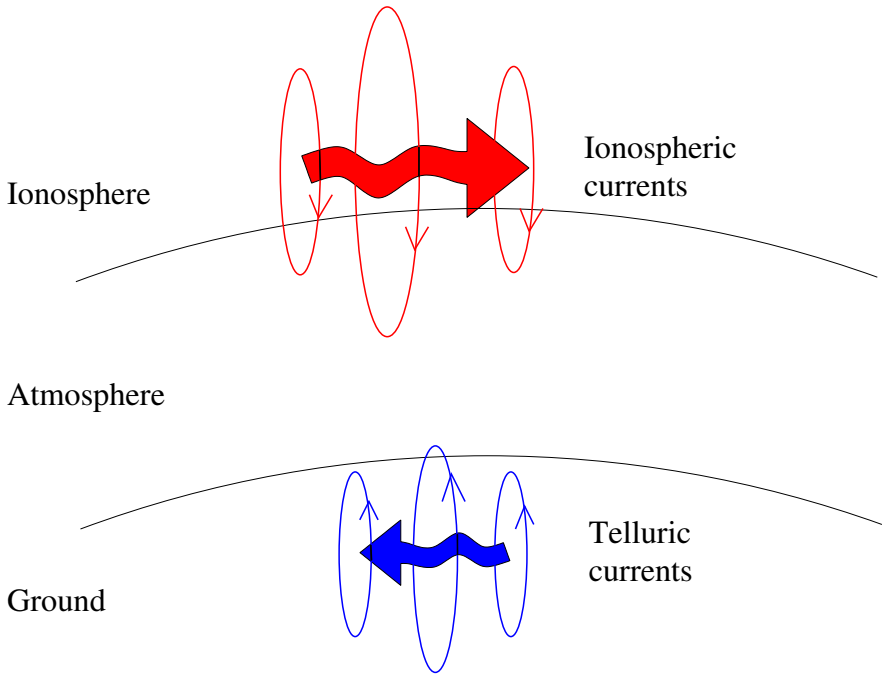

Figure 4.5: Schematic representation of the inductive coupling between the ionosphere and ground. Temporal changes in ionospheric currents and associated magnetic fields create an inductive electric field in the ground. This electric field drives the telluric currents, which create their own time-varyign magnetic fields.

situation is schematically illustrated in Fig. 4.5. The effects of the ground induced currents on magnetic measurements have been known for a long time, and have been extensively studied (e.g. Chapman and Bartels, 1940; Rikitake and Honkura, 1985; Tanskanen et al., 2001; Häkkinen et al., 2002). The methods used to extract the ground induced signal from the magnetic measurements are discussed in Section 3.1. Ground induction, associated with either natural magnetic variations or geomagnetic sounding, can also be used to investigate the conductivity structure of the Earth (e.g. Rikitake and Honkura, 1985; Olsen, 1999; Korja et al., 2002). Ground induction has to be taken into account also when studying geomagnetically induced currents (GIC) in man-made conductor systems, such as electric transmission lines and pipelines (e.g. Pirjola, 2002; Viljanen et al., 2004).

In all studies cited above the ground induced electric field is investigated only at the surface of the Earth, not at the ionosphere. In these studies the ionospheric (equivalent) currents are assumed to be known: If inductive coupling between the ionosphere and ground affects the ionospheric currents, these effects are assumed

to be included in the given current system (Pirjola, 1982). In Paper III we calculated the ionospheric effects of the secondary induced electric field[2] produced by ground induction. These calculations were somewhat approximative, as the ionospheric electric field was calculated as if in vacuum (see discussion in Section 4.2) and we also used simple 1-dimensional layered conductivity models of the Earth. The latter approximation allowed us to use the complex image method (CIM, Thomson and Weaver, 1975; Boteler and Pirjola, 1998) for modeling the ground induction. Calculations with more realistic Earth conductivity models would require far more sophisticated methods (e.g. Pulkkinen and Engels, 2005). Despite these approximations, the results obtained in Paper III should give the right magnitude for the ground induction effects in ionospheric electrodynamics.

In Paper III we studied the inductive coupling between the ionosphere and solid earth for some realistic models of typical ionospheric events, including WTS and Ω-bands. We concluded that the secondary induced electric field due to ground induction is quite small and uniformly distributed at ionospheric altitudes. The maximum magnitude of the secondary electric field was always $<$0.4 mV/m in the examples studied. This is an order of magnitude smaller than the potential electric field present at the same locations and 3-5 times smaller than the primary induced electric field created by ionospheric self-induction. Consequently, in Papers IV and V we concentrated on modeling only the ionospheric self-induction part.

Despite having only a small effect on electric fields at ionosphere, In Paper III we found that ground induction does modify the magnetic field even at satellite altitudes, ~ 400 km above the surface. At these altitudes the contribution from ground induced currents to the z-component of the magnetic field may be 30-40% of the total field. The horizontal magnetic field is dominated by FAC, so in that component the contribution from ground induction is insignificant. This should be considered when interpreting magnetic measurement from low-orbiting satellites.

Also other authors have considered the effect of ground induction on ionospheric electrodynamics. For example, Yoshikawa and Itonaga (1996) represented the Earth as a perfect conductor at some distance d below the ionosphere in their Alfvén wave reflection model that was discussed in Section 4.1. These results were used in Paper IV as a check for our own calculation method. Because we did not include ground induction in our model, the results by Yoshikawa and Itonaga (1996) were also modified accordingly (see appendix A of Paper IV). In Fig. 4.6 we plot the shear wave$\rightarrow$shear wave and shear wave$\rightarrow$fast wave reflection coefficients as functions of the horizontal wavelength (see discussion in Section 4.1, especially 4.1.1). The reflection coefficients are plotted for three cases: without

[2]In nomenclature of Paper III the electric field created by ionospheric self-induction is the primary induced field

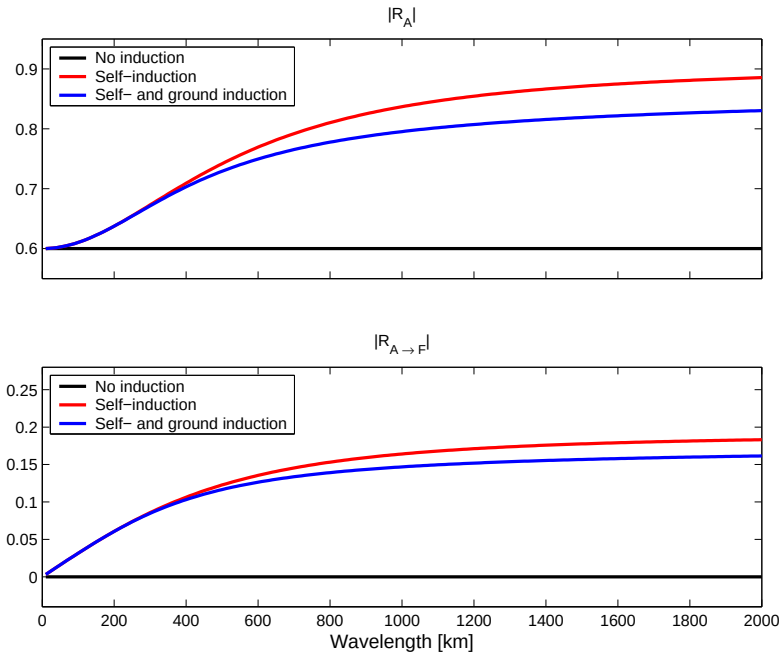

Figure 4.6: Absolute values of the reflection coefficients for shear Alfvén wave as functions of horizontal wavelength λ. Upper panel gives the reflection coefficient R_A (shear wave→shear wave) without any induction (black), with only ionospheric self-induction (red) and with also ground induction (blue). Lower panel gives the corresponding coefficient $R_{A\to F}$ (shear wave→fast wave). In this example ionospheric conductances $\Sigma_P = 4$ S and $\Sigma_H = 8$ S as well as frequency $\omega = 1$ s^{-1} and Alfvén conductance $\Sigma_A = 1$ S are held fixed, while λ is varied. See text for further discussion.

any induction (Eq. 4.3), with only ionospheric self-induction (Appendix A of Paper IV) and with both ionospheric and ground induction (Yoshikawa and Itonaga, 1996). We see that ionospheric self-induction modifies the reflection coefficient significantly even at small length scales (difference between black and red lines). On the other hand, the contribution from ground induction is observable only at wavelengths larger than ~ 500 km (difference between red and blue lines). Even at the longer wavelengths ionospheric self-induction affects the reflection coefficients more than the ground induction. It should also be noted that ground induction opposes the changes caused by ionospheric self-induction. This is expected, as the ground induced currents exactly cancel all variations of the horizontal electric field at the surface of the (supposedly) perfectly conducting ground.

The smoothness of the secondary electric field found in Paper III and the dependence on horizontal wavelength demonstrated in Fig. 4.6 are quite natural, and can be understood with a simple consideration of the potential theory. If we assume that there are no free charges or electric currents in the neutral atmosphere, we have

$$\nabla \cdot \boldsymbol{E} = 0, \tag{4.10}$$

$$\nabla \times \boldsymbol{E} = -\frac{\partial \boldsymbol{B}}{\partial t}, \tag{4.11}$$

$$\nabla \times \boldsymbol{B} = 0. \tag{4.12}$$

Taking the curl of Faraday's law and using the other two equations it follows that

$$\nabla^2 \boldsymbol{E} = 0 \tag{4.13}$$

holds in the neutral atmosphere. The above result means that if the electric field is known at some altitude $z = h$, each vector component can be separately upward or downward continued in Fourier presentation as

$$\tilde{E}_*(k_x, k_y, z) = \tilde{E}_*(k_x, k_y, h)\, e^{\pm\sqrt{k_x^2+k_y^2}(z-h)} \tag{4.14}$$

Here k_x, k_y are the horizontal wavenumbers, $* \in \{x, y, z\}$ and $\tilde{E}_*$ is the horizontal Fourier-transform of E_*. The plus sing in the exponent is for the ground induced electric field, while the minus sign is for ionospheric induction.

The primary electric field created by ionospheric self-induction is often quite structured (see e.g. Fig. 5 in Paper III). However, when it is downward continued from the ionosphere to the surface of the Earth, small scale variations are heavily suppressed, according to Eq. (4.14). Ground induction creates the secondary induced field that (partly) cancels the primary field at the surface. When the secondary field is upward continued back to the ionosphere, the result is a very smooth field, as in Fig. 5 of Paper III. The heavy suppression of small wavelengths also explains why ground induction modifies Alfvén wave reflection only at the largest horizontal scales. The models studied in Paper III were quite localized, so the contribution from ground induction was negligible.

Chapter 5

Summary, conclusions and outlook

Ionospheric electrodynamics has an important role in the Solar-Terrestrial research. Especially the auroral ionospheres are key regions, where magnetosphere-ionosphere coupling can be studied in detail. In this thesis we have focused on theoretical modeling of ionospheric electrodynamics, especially at high magnetic latitudes and during dynamical events. Also keeping in mind the spatial extent of the MIRACLE instrument network (see Fig. 2.1) we have concentrated on mesoscale studies, covering areas of a few hundred to a few thousand km across. During the thesis work we have developed two new analysis methods to be used with different ground-based measurements and a new model for describing inductive processes taking place in the ionosphere.

In Paper I we developed the 1-dimensional spherical elementary current method (1D SECS) for deriving ionospheric equivalent currents from ground based magnetic measurements along a meridional magnetometer chain. This is the first 1-dimensional upward continuation method that can be used both at local and global scales and also takes the spherical geometry of the ionosphere correctly into account. The comparisons made in Paper I using both synthetic and real data show that the new 1D SECS method is more accurate than the earlier 1D Fourier method by Mersmann et al. (1979). We also conclude that the integrated total currents flowing across the magnetometer chain given by the 1D SECS method would give a better characterization of magnetic activity than the local IU and IL indices. Errors in the 1D SECS results are generally 5-10% in the current density profiles along the magnetometer chain and $\sim$5% in integrated total currents. The 1D SECS method is especially suitable for analyzing electrojet situations, which are inherently 1-dimensional. However, the tests performed using real data indicate that the 1D SECS method works well also in more complicated situations.

In Paper II we re-analyzed the problem of determining ionospheric electric fields and currents using ground magnetic measurements and ionospheric conductivity estimates as the input data. Our motivation for this was the fact that the

standard KRM solution developed by (Kamide et al., 1981) does not work well in local scales (Murison et al., 1985). The KRM method does work in global scales, but when applied to smaller regions the solution depends strongly on the unknown boundary conditions at the borders of the analysis area. The new CECS-based analysis technique developed in Paper II differs from the traditional KRM method in two key points: 1) The primary unknown to be solved is the curl-free part of the currents instead of the electric potential, resulting in more efficient use of the input data. 2) The "no sources outside analysis area" -boundary condition is implicitly included in the solution. These new features make our new calculation method less prone to errors in regional studies, which was demonstrated in several realistic model situations. In these tests the errors in the results of the CECS-based method were 20-40%, whereas the traditional KRM method was less accurate. In Section 3.2.1 we demonstrated the effect of different ionospheric conductance estimates on the CECS-based solution. We found that the electric field is affected most by the conductance model, whereas the horizontal and field-aligned currents are somewhat less sensitive. Similar behavior is expected with the traditional KRM method (Kamide et al., 1981).

The role of induction in the ionospheric electrodynamics was studied in Papers III-V. In Paper III we made approximative calculations which allowed us to conclude that the inductive coupling between the solid earth and ionosphere is not important in the context of ionospheric electric fields. However, ground induction does modify the magnetic field even at low satellite orbits. We also concluded that internal induction in the ionosphere may produce significant rotational electric fields. In Paper IV we developed a new and self-consistent method for solving induced electric fields using ionospheric conductances and potential part of the electric field as the input data. The new calculation method is based on the elementary current systems and it is unique in that purely ionospheric parameters are used as input. This is in contrast to the previous Alfvén-wave studies discussed in Section 4.1.1. In Paper V the new calculation method was applied to several realistic models of ionospheric electrodynamics. We found that the induced electric field is important at local "hot-spots", reaching values 20-50% of the potential electric field present at the same locations. Also the induced FAC make a large contribution to the total field-aligned currents flowing between the ionosphere and magnetosphere. These results demonstrate that in dynamical situations ionospheric electric fields cannot be modeled as simple potential fields, like done in many occasions (also in the analysis method developed in Paper II). In addition to the exact calculations, In Paper V and in Section 4.2 we also present approximate formulas for estimating the magnitude of the induced electric field from typical conductances and length and time scales, and the shape of the induced field from time derivatives of the equivalent currents.

The unifying theme in the above studies is the use of elementary current sys-

tems for describing ionospheric electric fields and currents. The theoretical basis of the calculation methods developed in Papers I-V can be formulated without elementary current systems and in principle any numerical method could be used in the actual calculations. However, elementary currents form a convenient set of basis functions for describing 2-dimensional (or 1-dimensional) vector fields in terms of their divergences and curls. The fact that already the basis functions are either divergence- or curl-free is very natural in ionospheric electrodynamics: Equivalent currents are divergence-free, curl-free currents are (approximately) magnetically invisible below the ionosphere and inductive electric fields are divergence-free. Also the way boundary conditions are handled in the methods developed in Papers II and IV highlights the usefulness of the elementary current systems.

5.1 Future directions

The results presented in the thesis open several opportunities for future research projects. In fact, the 1D SECS method has already been generalized by Juusola et al. (2006) to be used with satellite measurements. Some other possible research topics are considered below.

1) In Paper I the 1D SECS method was used to determine the ionospheric equivalent currents directly from ground magnetic measurements, without separating the measured field into internal and external parts. The results obtained by Juusola et al. (2006) would allow us to model also the internal currents with 1D SECS, and thus separate the measured field. The existing 1-dimensional separation methods do not take the spherical geometry properly into account on local scales (e.g. Untiedt and Baumjohann, 1993), and the 2-dimensional methods require a very dense magnetometer network (e.g. Pulkkinen et al., 2003b). The 1D SECS separation method would handle the geometrical issues correctly, could be used in local and global studies and might also be more robust than the 2-dimensional methods with respect to input data coverage. As mentioned in Section 3.1.3, the 1D SECS method is simple and fast enough that it could be used to replace the local IU and IL indices. Even more reliable estimates of the ionospheric electrojet activity could be achieved by including the separation of the internal and external parts of the magnetic field in the analysis.

2) In the CECS-based solution method developed in Paper II we use the ionospheric equivalent currents and conductance estimates as the input data. In the tests performed in Paper II we conclude that the error in the resolved electric field and current distributions is 20-40%, even when we use the correct conductances

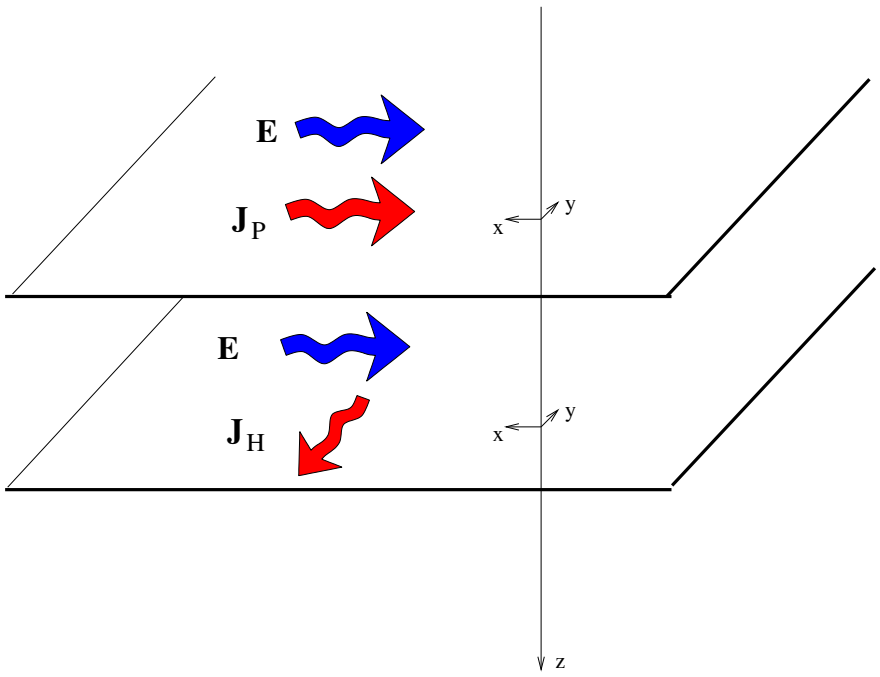

Figure 5.1: Schematic illustration of the 2-sheet ionospheric model. The upper sheet would contain mainly Pedersen currents and the lower sheet mainly Hall currents.

as input. The solution might be improved, if we have some additional information about the ionospheric electric field. For example, point measurements of the electric field by the EISCAT radars [6] could be used as constraints in the calculations. Such constrained solutions could improve the accuracy of the solutions, at least near the location of the constraint. However, it should be kept in mind that in practical studies also the input conductances may contain large errors, as discussed in Section 3.2.1.

3) In this thesis we have used the thin-sheet approximation in the ionosphere, i.e. we have assumed that all horizontal currents flow within an infinitely thin sheet at some fixed altitude above the ground. The thin sheet approximation simplifies the analysis, but it is not always a sufficiently accurate description of the ionosphere. Especially in induction studies the altitude resolved ionosphere could add new features to the solution. The next step into this direction would be to describe the ionosphere with two thin sheets placed at different altitudes, as in Fig. 5.1. The upper sheet would contain mainly Pedersen currents, while the ma-

jority of Hall currents would flow at the lower sheet. This approximation is based on the fact that ionospheric Pedersen and Hall conductances peak at slightly different altitudes, as is the case also in Fig. 1.3. Already this simple model would include several new features, such as the possibility of vertical closure of current within the ionosphere and inductive coupling between the current sheets.

4) Another interesting possibility for generalizing the inductive calculation method developed in Paper IV would be to construct an inductive ionospheric solver for a global magnetospheric MHD simulation. The method developed in Paper IV requires ionospheric conductances and the potential part of the electric field as the input data. However, most global MHD simulations give the FAC and conductances as input to their ionospheric solvers (Janhunen, 1998). The reason is that this procedure is easier to implement in the magnetospheric side of the simulation. In principle it should be possible to reformulate the calculation method of Paper IV so that the FAC (or the curl-free part of the horizontal current) is used as input instead of the potential part of the electric field. In this approach the MHD simulation would give the conductances and FAC for the ionospheric solver, and the solved electric field (which would now have an inductive part) would be mapped back to the magnetosphere and used as a boundary condition in the MHD simulation. The practical feasibility of this approach and the possible impacts ionospheric induction may have on ionosphere-magnetosphere coupling remain to be seen.

Appendix A

How to use elementary current systems

In the thesis we have used special vector basis functions called elementary current systems quite extensively, as they formed the basis of the numerical calculation methods used in Papers I-V. This Appendix is meant to be a general introduction to the use of the elementary current systems, so that the various bits of information presented in the research articles are gathered in one place.

Elementary current systems (ECS) were introduced by Amm (1997). Although their name refers to currents, they can be used to represent any smooth enough (continuously differentiable) 2-dimensional vector field. Elementary current systems can be defined either in spherical or Cartesian geometry, and they are called SECS and CECS, respectively. There are two different types of ECS, one is divergence-free (DF) and the other curl-free (CF). Together they form a complete set of basis functions for representing 2-dimensional vector fields on a sphere (SECS) or on a plane (CECS). Here we will concentrate on CECS, but SECS can be used in a completely analogous manner.

CECS

CECS are defined so that they have cylindrical symmetry, and either a δ-function curl or divergence at their origin. This uniquely determines the DF and CF CECS, which can be written out as (misprint in Eq. (4) of Amm,1997, is corrected here)

$$\boldsymbol{J}^{cf} = \frac{I^{cf}}{2\pi\rho'}\,\hat{\boldsymbol{e}}_{\rho_p}. \tag{A.1}$$

$$\boldsymbol{J}^{df} = \frac{I^{df}}{2\pi\rho'}\,\hat{\boldsymbol{e}}_{\phi_p} \tag{A.2}$$

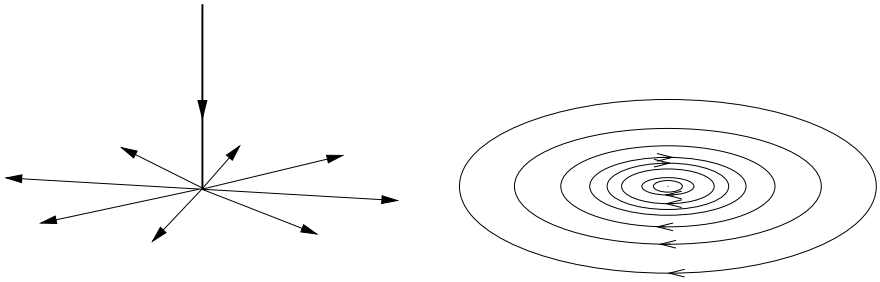

Figure A.1: Curl-free (CF) and divergence-free (DF) Cartesian elementary current systems (CECS).

Here $\rho' = \sqrt{(x - x_p)^2 + (y - y_p)^2}$ is the horizontal distance between the observation point (x, y) and the CECS pole located at (x_p, y_p). The unit vectors $\hat{\boldsymbol{e}}_{\phi_p}$ and $\hat{\boldsymbol{e}}_{\rho_p}$ are given in the cylindrical coordinate system centered at the CECS pole. Constants I^{cf} and I^{df} are called the scaling factors of the CF and DF CECS, respectively. In Papers I-V we use the convention that scaling factors of CECS representing currents are denoted with I^{cf}, I^{df} and those representing electric fields are denoted with V^{cf}, V^{df}.

The elementary systems are defined in such a way, that the CF CECS has a Dirac δ-function divergence and the DF CECS a δ-function curl at its pole,

$$\nabla \cdot \boldsymbol{J}^{cf} = I^{cf}\, \delta(x - x_p)\, \delta(y - y_p)$$

$$(\nabla \times \boldsymbol{J}^{df})_z = I^{df}\, \delta(x - x_p)\, \delta(y - y_p).$$

When CECS are used to represent ionospheric currents, the divergence of the CF CECS at its pole is interpreted as a vertically flowing FAC,

$$j_{\parallel}^{cf} = I^{cf} \delta(x_p - x)\, \delta(y_p - y)\, U(z_p - z). \tag{A.3}$$

Here $U(z_p - z)$ is the Heaviside unit step function. CECS are illustrated in Fig. A.1, while corresponding SECS appear in Fig. 1 of Paper I. In these figures also the FAC are included.

It should be emphasized that Eqs. (A.1) and (A.2) give the vector fields only at the ionospheric plane. When CECS are used to represent ionospheric sheet currents, the altitude dependence is a δ-function at the ionospheric height. This is explicitely written out in Eqs. (1) and (2) of Paper IV. On the other hand, when CECS are used to represent the electric field, we assume that the field has the same magnitude at all altitudes.

Electric fields and currents with CECS

By placing a sufficient number of CF and DF CECS at different locations of the plane, one can construct any 2-dimensional vector field from its sources and curls, in accordance with Helmholtz's theorem. In practical calculations the CECS are placed at some discrete grid, and the scaling factors give the divergence and curl of the vector field in the grid cell. For some arbitrary grid cell k

$$I_k^{cf} = \int_{cell\ k} \nabla \cdot \boldsymbol{J}\, \mathrm{da}, \tag{A.4}$$

$$I_k^{df} = \int_{cell\ k} (\nabla \times \boldsymbol{J})_z\, \mathrm{da}. \tag{A.5}$$

This means that the curl and divergence that are in reality distributed over the grid cell are represented by point sources at the middle of the cell. In numerical calculations we have used regular rectangular grids, although in principle any grid structure would be possible.

The numerical values of the vector field represented by the CECS can be calculated at any desired location using Eqs. (A.1) and (A.2). However, one should be careful not to calculate vector values too close to the CECS poles, as the fields are singular there. This does cause some inconvenience, but in practice we have avoided numerical problems by calculating the vector values only at the corners of the CECS grid cells. This way Eqs. (A.1) and (A.2) are ussed only outside those grid cells where the CECS are situated. If it is necessary to calculate the fields inside the grid cells, we may subdivide the cells into smaller units and proceed as before.

The CECS are placed at some discrete grid and the vector values are calculated at another set of grid points. Our notation here[1] is such that the 2-dimensional vector fields (in this example the ionospheric electric field) are indicated using bold italics, $\boldsymbol{E}$. The collection of the x- and y-components of the field $\boldsymbol{E}$ at all grid points is written in script style, as $\boldsymbol{\mathcal{E}}$, and can be written out as

$$\boldsymbol{\mathcal{E}} = \left[E_x(\boldsymbol{r}_1),\, E_y(\boldsymbol{r}_1),\, E_x(\boldsymbol{r}_2),\, \ldots,\, E_y(\boldsymbol{r}_N)\right]^T. \tag{A.6}$$

Here $E_x(\boldsymbol{r}_n)$ is the x-component of $\boldsymbol{E}$ at the grid point $\boldsymbol{r}_n$, and so on. In a similar fashion the collection of the CECS scaling factors representing the field $\boldsymbol{E}$ is indicated using fraktur style, $\mathfrak{V}$, and is defined as

$$\mathfrak{V} = \left[V^{cf}(\boldsymbol{r}_{p1}),\, V^{df}(\boldsymbol{r}_{p1}),\, V^{cf}(\boldsymbol{r}_{p2}),\, \ldots,\, V^{df}(\boldsymbol{r}_{pM})\right]^T. \tag{A.7}$$

[1] Unfortunately several different notations are used in Papers I-V. We apologize.

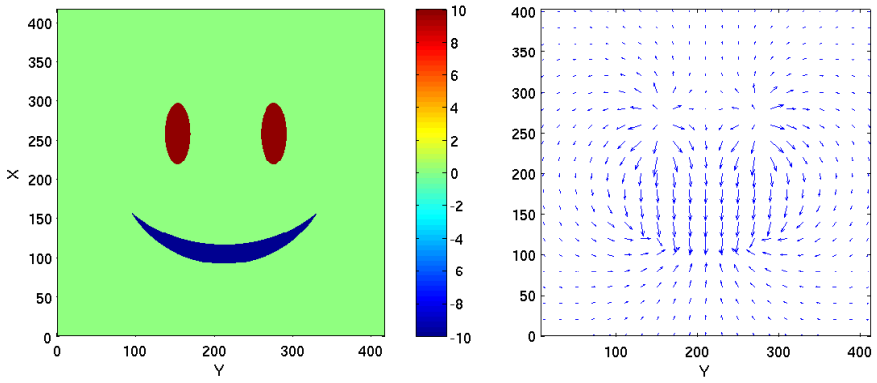

Figure A.2: On the left scaling factors of CF CECS, and on the right the corresponding vector field. Scaling factors, vector values and lengths are in arbitrary units.

Here $V^{cf}(\boldsymbol{r}_{pm})$ is the scaling factor of the curl-free CECS located at grid point $\boldsymbol{r}_{pm}$. There is a linear relation between the vector components and the CECS scaling factors,

$$\boldsymbol{\mathcal{E}} = \mathrm{M} \cdot \mathfrak{V}. \tag{A.8}$$

The transfer matrix M depends only on the geometry of the vector and CECS grids, and can be calculated using Eqs. (A.2) and (A.1). For example, in the above numbering scheme $M_{1,1}$ gives that part of the x-component of $\boldsymbol{E}$ at position $\boldsymbol{r}_1$ that is caused by the CF CECS located at $\boldsymbol{r}_{p1}$. It can be written out as

$$M_{1,1} = \frac{1}{2\pi} \frac{x_1 - x_{p1}}{(x_1 - x_{p1})^2 + (y_1 - y_{p1})^2} \tag{A.9}$$

Similarly, $M_{2,1}$ gives E_y at $\boldsymbol{r}_1$ caused by CF CECS located at $\boldsymbol{r}_{p1}$, $M_{3,2}$ gives E_x at $\boldsymbol{r}_2$ caused by DF CECS located at $\boldsymbol{r}_{p1}$ and so on.

A potential field can be modeled with just CF CECS. In this case those parts of the vector $\mathfrak{V}$ and matrix M that correspond to DF CECS are omitted. Figure A.2 shows an example of a CF CECS distribution and corresponding vector field. In a similar manner, a purely rotational field can be constructed using only DF CECS. Equation (A.8) can also be inverted, so that the CECS scaling factors are determined when the vector field is known. This is a convenient way of dividing a given vector field into curl-free and divergence-free parts. If the vector field is specified only inside a limited region, it may contain a Laplacian part that has a zero curl and divergence inside the region. For this reason the CECS grid should be slightly larger than the area of interest, so that the Laplacian part of the vector field may be modeled with the outermost CECS. This is illustrated in Fig. A.3.

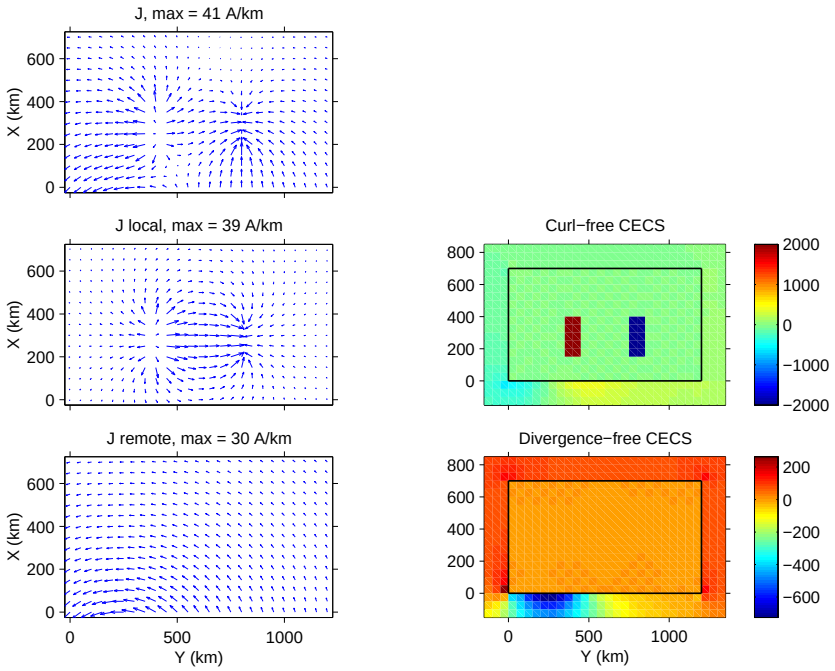

Figure A.3: An example of representing a given vector field with CECS. Left side: The total current system, the local part of the currents and the remote part of the current. Right side: The distributions of curl- and divergence-free CECS that correspond to the total current system. The black rectangle marks the area where the vector values are plotted. See text for further details.

The total current system consist of an irrotational local part and a divergence-free remote part. The vector field given in the figure is decomposed using CECS, the local part is correctly represented in terms of CF CECS inside the area where the vector field was originally specified (marked with a black rectangle). The remote part is represented in terms of both CF and DF CECS placed just outside this area.

Magnetic fields of elementary currents

The magnetic fields of the current distributions given in in Eqs. (A.1)-(A.3) can be calculated by a straightforward integration of the vector potential (Amm and Viljanen, 1999; Pirjola and Viljanen, 1998, and Paper III),

$$\boldsymbol{B}^{cf} = \frac{\mu_0 I^{cf}}{2\pi\rho'} U(z_p - z)\, \hat{\boldsymbol{e}}_{\phi_p}, \tag{A.10}$$

$$\boldsymbol{B}^{df} = \frac{\mu_0 I^{df}}{4\pi\rho'} \left(\left[1 - \frac{|z - z_p|}{\sqrt{\rho'^2 + (z - z_p)^2}} \right] \operatorname{sign}(z - z_p)\, \hat{\boldsymbol{e}}_{\rho_p} + \frac{\rho'}{\sqrt{\rho'^2 + (z - z_p)^2}}\, \hat{\boldsymbol{e}}_z \right). \tag{A.11}$$

The divergence-free system with associated FAC does not produce any magnetic field below the ionosphere, in accordance with Fukushima's theorem (Fukushima, 1976).

As explained in Section 3.1, the magnetic variations at ground can be explained in terms of divergence-free equivalent currents. The magnetic field of a given DF CECS configuration can be calculated as

$$\boldsymbol{\mathcal{B}} = \mathrm{M}_B \cdot \boldsymbol{\mathfrak{I}}^{df}. \tag{A.12}$$

Here $\boldsymbol{\mathcal{B}}$ is a vector of magnetic field values similar to Eq. (A.6), $\boldsymbol{\mathfrak{I}}^{df}$ is a vector of DF CECS scaling factors similar to Eq. (A.7) and M_B is a relation matrix. The matrix M_B depends just on the geometry of the situation and can be calculated using Eq. (A.11) in a similar way as M in Eq. (A.8).

The equivalent current distribution is obtained by inverting Eq. (A.12). More detailed discussion of the equivalent currents in general and the elementary current method in particular can be found in Amm and Viljanen (1999), Pulkkinen et al. (2003a,b) and Paper I.

Bibliography

[1]: http://modelweb.gsfc.nasa.gov/
ModelWeb, different models of the near Earth space environment. Maintained by the Space Physics Data Facility of the NASA Goddard Space flight Center. Last accessed on 18.6.2007.

[2]: http://en.wikipedia.org/
English version of the free encyclopedia Wikipedia. Maintained by the Wikimedia Foundation. See e.g. articles on "Aurora", "Ionosphere", "Magnetosphere" and links therein. Last accessed on 18.6.2007.

[3]: http://www.oulu.fi/ spaceweb/textbook/
Oulu Space Physics Textbook. Maintained by the Space Physics Group, University of Oulu. Last accessed on 18.6.2007.

[4]: http://swdcwww.kugi.kyoto-u.ac.jp/
World Data Center for Geomagnetism at Kyoto. Maintained by the Data Analysis Center for Geomagnetism and Space Magnetism, Kyoto University. Last accessed on 18.6.2007.

[5]: http://space.fmi.fi/MIRACLE/
MIRACLE instrument network. Site is maintained by the Space Research group of the Finnish Meteorological Institute. Last accessed on 18.6.2007.

[6]: http://www.eiscat.com/
EISCAT (European Incoherent Scattter) radar system. Maintained by the EISCAT Scientific Association. Last accessed on 18.6.2007.

[7]: http://superdarn.jhuapl.edu/
SuperDARN, an international ionospheric radar network. Site is maintained by the Applied Physics Laboratory of the Johns Hopkins University. Last accessed on 18.6.2007.

[8]: http://www.intermagnet.org/
INTERMAGNET, International Real-time Magnetic Observatory Network. Last accessed on 18.6.2007.

[9]: http://www.wdc.bgs.ac.uk/ // World Data Centre for Geomagnetism at Edinburgh. Site is maintained by the British Geological Survey. Last accessed on 18.6.2007.

[10]: http://www.ngdc.noaa.gov/
National Geophysical Data Center. Site is maintained by National Oceanic & Atmospheric Administration (NOAA) of the United States. Last accessed on 18.6.2007.

[11]: http://web.dmi.dk/fsweb/projects/chain/
Greenland magnetometer chain. Site is maintained by the Danish Meteorological Institute. Last accessed on 18.6.2007.

[12]: http://stdb2.stelab.nagoya-u.ac.jp/mm210/
210 magnetic meridian network. Site is maintained by the Solar-Terrestrial Environment Laboratory, Nagoya university. Last accessed on 18.6.2007.

[13]: http://ethesis.helsinki.fi/
Electronic versions of doctoral dissertations and other publications from the University of Helsinki. Last accessed on 18.6.2007.

Ahn B.-H., R. M. Robinson, Y. Kamide and S.-I. Akasofu, "Electric conductivities, electric fields and auroral particle energy injection rate in the auroral ionosphere and their empirical relations to the horizontal magnetic disturbances", *Planet. Space Sci.*, **31**, 641–653, 1983.

Ahn B.-H., A. D. Richmond, Y. Kamide., et al., "An ionospheric conductance model based on ground magnetic disturbance data", *J. Geophys. Res.*, **103**, 14769–14780, 1998.

Akasofu S.-I., "The development of the auroral substorm", *Planet. Space Sci.*, **12**, 273–282, 1964.

Akasofu S.-I. and D. S. Kimball, "The dynamics of the aurora - I Instabilities of the aurora", *J. Atm. Terr. Phys.*, **26**, 205–211, 1964.

Akasofu S.-I., D. S. Kimball and C.-I. Meng, "The dynamics of the aurora - II Westward traveling surges", *J. Atm. Terr. Phys.*, **27**, 173–187, 1965.

Aksnes A., O. Amm, J. Stadsnes et al., "Ionospheric conductances derived from satellite measurements of auroral UV and X-ray emissions, and ground-based data: A comparison", *Ann. Geophys.*, **23**, 343–358, 2005.

Amm O., "Direct determination of the local ionospheric Hall conductance distribution from two-dimensional electric and magnetic field data: Application of the method using models of typical ionospheric electrodynamic situations", *J. Geophys. Res.*, **100**, 21473–21488, 1995.

Amm O., "Improved electrodynamic modeling of an omega band and analysis of its current system", *J. Geophys. Res.*, **101**, 2677–2683, 1996.

Amm O., "Ionospheric elementary current systems in spherical coordinates and their application", *J. Geomagnetism and Geoelectricity*, **49**, 947–955, 1997.

Amm O., "Method of characteristics in spherical geometry applied to a Harang-discontinuity situation", *Ann. Geophys.*, **16**, 413–424, 1998.

Amm O. and A. Viljanen, "Ionospheric disturbance magnetic field continuation from the ground to the ionosphere using spherical elementary current systems", *Earth, Planets and Space*, **51**, 431–440, 1999.

Amm O., "The elementary current method for calculating ionospheric current systems from multisatellite and ground magnetometer data", *J. Geophys. Res.*, **106**, 24843–24855, 2001.

Amm O., "Method of characteristics for calculating ionospheric electrodynamics from multisatellite and ground-based radar data", *J. Geophys. Res.*, **107** (A10), 1270, doi:10.1029/2001JA005077, 2002.

Amm O., M. Engebretson, T. Hughes, L. Newitt, A. Viljanen and J. Watermann, "A traveling convection vortex event study: Instantaneous ionospheric equivalent currents, estimation of field-aligned currents, and the role of induced currents", *J. Geophys. Res.*, **107** (A11), 1334, doi:10.1029/2002JA009472, 2002.

Amm O., A. Viljanen, A. Pulkkinen, I. Sillanpää and H. Vanhamäki, "Methods for combined ground-based and space-based analysis of ionospheric current systems", *Proc. Fourth Oersted International Science Team Conference, Copenhagen, Denmark, Sep 23-27, 2002*, 181–184, 2003.

Amm O., E. F. Donovan, H. Frey et al., "Coordinated studies of the geospace environment using Cluster, satellite and ground-based data: An interim report", *Ann. Geophys.*, **23**, 2129–2170, 2005.

Baker D. N., T. I. Pulkkinen, V. Angelopoulos, W. Baumjohann and R. L. McPherron, "Neutral line model of substorms: Past results and present view", *J. Geophys. Res.*, **101**, 12975–13010, 1996.

Baumjohann W. and R. Treumann, "Basic space plasma physics", ISBN 1-86094-079-X, *Imperial College Press*, London, 1997.

Bilitza D., "International reference ionosphere 2000", *Radio Sci.*, **36**, 261–275, 2001.

Boteler D. and R. Pirjola, "The complex-image method for calculating the magnetic and electric fields produced at the surface of the Earth by the auroral electrojet, *Geophys. J. Int.*, **132**, 31–40, 1998.

Browne S., J. K. Hargreaves and B. Honary, "An imaging riometer for ionospheric studies", *Electronics & Communication Engineering J.*, **7**, 209–217, 1995.

Buchert S., "Magneto-optical Kerr effect for a dissipative plasma", *J. Plasma Phys.*, **59**, 39–55, 1998.

Buchert S., and F. Budnik, "Field-aligned current distribution generated by a divergent Hall current", *Geophys. Res. Lett.*, **24**, 297–300, 1997.

Campbell W., "An introduction to quiet daily geomagnetic fields", *Pure and Applied Geophysics*, **131**, 315–331, 1989.

Campbell W., "Introduction to Geomagnetic fields", ISBN 0-521-57193-6, *Cambridge University Press*, Cambridge, 1997.

Chapman S. and J. Bartels, "Geomagnetism, vol. II", *Oxford University Press*, New York, 1940.

Cowley S. W. H., "Magnetosphere-ionosphere interactions: A tutorial review", pp. 91–106 in Ohtani et al. (2000).

Davies K., "Ionospheric Radio", ISBN 0-86341-186-X, *Peter Peregrinus*, London, 1996.

Dungey J. W., "Interplanetary magnetic field and the auroral zones", *Phys. Rew. Lett.*, **6**, 47–48, 1961.

Fukushima N., "Generalized theorem for no ground magnetic effect of vertical currents connected with Pedersen currents in the uniform-conductivity ionosphere", *Rep. Ionos. Space. Res. Japan*, **30**, 35–40, 1976.

Fuller-Rowell T. J. and D. S. Evans, "Height-integrated Pedersen and Hall conductivity patterns inferred from the TIROS-NOAA satellite data", *J. Geophys. Res.*, **92**, 7606–7618, 1987.

Glassmeier K.-H., "On the influence of ionospheres with non-uniform conductivity distribution on hydromagnetic waves", *J. Geophys.*, **54**, 125–137, 1984.

Gonzalez W. and B. Tsurutani, "Criteria of interplanetary parameters causing intense magnetic storms (Dst $<$ -100 nT)", *Planet. Space Sci.*, **35**, 1101–1109, 1987.

Gonzalez W., J. A. Joselyn, Y. Kamide et al., "What is a geomagnetic storm", *J. Geophys. Res.*, **99**, 5771–5792, 1994.

Greenwald R., K. Baker, J. Dudeney at al., "DARN/SuperDARN: A global view of the dynamics of high latitude convection", *Space Sci. Rev.*, **71**, 761–796, 1995.

Greifinger C. and P. Greifinger, "Theory of hydromagnetic propagation in the ionospheric waveguide", *J. Geophys. Res.*, **73**, 7473–7490, 1968.

Haines G. V., "Spherical cap harmonic analysis", *J. Geophys. Res.*, **90**, 2583–2591, 1985.

Hughes W.J., and D. Southwood, "The screening of micropulsation signals by the atmosphere and ionosphere", *J. Geophys. Res.*, **81**, 3234–3240, 1976.

Huttunen E., "Interplanetary shocks, magnetic clouds and magnetospheric storms", PhD thesis, *Finnish Meteorological Institute Contributions*, **48**, 2005. Electronic version is available at [13].

Huttunen E., H. Koskinen, T. Pulkkinen, A. Pulkkinen, M. Palmroth, G. Reeves and H. Singer, "April 2000 magnetic storm: Solar wind driver and magnetospheric response", *J. Geophys. Res.*, **107** (A12), 1440, doi:10.1029/2001JA009154, 2002.

Häkkinen L., T. Pulkkinen, H. Nevanlinna, R. Pirjola and E. Tanskanen, "Effects of induced currents on Dst and on magnetic variations at midlatitude stations", *J. Geophys. Res.*, **107** (A1), 1014, doi:10.1029/2001JA900130, 2002.

Ieda A. and Y. Kamide, "Real-time modeling of the ionosphere using GEDAS/KRM for space weather", in *Proceedings of ISSS-7*, 26-31 March, 2005.

Iijima T., "Fiel-Aligned Currents in Geospace: Substance and Significance", pp. 107–129 in Ohtani et al. (2000).

Inhester B., J. Untiedt, M. Segatz and M. Kürschner, "Direct determination of the local ionospheric Hall and Pedersen conductance distributions from two-dimensional electric and magnetic field data", *J. Geophys. Res.*, **97**, 4073–4083, 1992.

Jakowski N., S. Heise, A. Wehrenpfennig, S. Schüter and R. Reimer, "GPS/GLONASS-based TEC measurements as a contributor for space weather forecast", *J. Atmos. Solar-Terr. Phys.*, **64**, 729–735, 2002.

Janhunen P., "On the possibility of using an electromagnetic ionosphere in global MHD simulations", *Ann. Geophys.*, **16**, 397–402, 1998.

Janhunen P., "Reconstruction of electron precipitation characteristics from a set of multi-wavelength digital all-sky auroral images", *J. Geophys. Res.*, **106**, 18505–18516, 2001.

Juusola L., O. Amm and A. Viljanen, "One-dimensional spherical elementary current systems and their use for determining ionospheric currents from satellite measurement", *Earth Planets Space*, **58**, 667–678, 2006.

Kamide Y., "The auroral electrojets: Relative importance of ionospheric conductivities, and electric fields", pp. 385–399 in Meng et al. (1991).

Kamide Y., E. A. Kihn, A. J. Ridley, E. W. Cliver and Y. Kadowaki, "Real-time specifications of the geospace environment", *Space Sci. Rev.*, **107**, 307–316, 2003.

Kamide Y., A. Richmond and S. Matsushita, "Estimation of ionospheric electric fields, ionospheric currents, and field-aligned currents from ground magnetic records", *J. Geophys. Res.*, **86**, 801–813, 1981.

Kamide Y. and A. Richmond, "Ionospheric conductivity dependence of electric fields and currents estimated from ground magnetic observations", *J. Geophys. Res.*, **87**, 8331–8337, 1982.

Kauristie, K., T. Pulkkinen, R. Pellinen and H. Opgenoorth, "What can we tell about global auroral-electrojet activity from a single meridional magnetometer chain?", *Ann. Geophys.*, **14**, 1177–1185, 1996.

Kersley L., S. E. Pryse, M. H. Denton et al., "Radio tomographic imaging of the northern high-latitude ionosphere on a wide geographical scale", *Radio Sci.*, **40**, RS5003, doi:10.1029/2004RS003103, 2004.

Kivelson M. and D. Southwood, "Resonant ULF waves: A new interpretation", *Geophys. Res. Lett.*, **12**, 49–52, 1985.

Kivelson M. and D. Southwood, "Coupling of global magnetospheric MHD eigenmodes to field line resonances", *J. Geophys. Res.*, **91**, 4345–4351, 1986.

Korja T., M. Engels, A. Zhamaletdinov et al., "Crustal conductivity in Fennoscandia - a compilation of a database on crustal conductance in the Fennoscandian Shield", *Earth Planets Space*, **54**, 535–558, 2002.

Lester M., J. A. Davies and T. S. Virdi, "High-latitude Hall and Pedersen conductances during substorm activity in the SUNDIAL-ATLAS campaign", *J. Geophys. Res.*, **101**, 26719–26728, 1996.

Lionheart W., "EIT Reconstruction Algorithms: Pitfalls, Challenges and Recent Developments", arXiv:physics/0310151v2 [physics.med-ph], at http://arxiv.org, 2004.

Lotko W., "Inductive magnetosphere-ionosphere coupling", *J. Atmos. Solar-Terr. Phys.*, **66**, 1443–1456, 2004.

Lu G., A. D. Richmond, J. M. Ruohoniemi, R. A. Greenwald, M. Hairston, F. J. Rich and D. S. Evans, "An investigation of the influence of data and model inputs on assimilative mapping of ionospheric electrodynamics", *J. Geophys. Res.*, **106**, 417–433, 2001.

Lühr H., A. Aylward, S. Buchert, K. Pajunpää, T. Holmboe and S. Zalewski, "Westward moving dynamic substorm features observed with the IMAGE magnetometer network and other ground-based instruments", *Ann. Geophys.*, **16**, 425–440, 1998.

Lui A. T. Y., "Current disruption in the Earth's magnetosphere: Observation and models", *J. Geophys. Res.*, **101**, 13067–13088, 1996.

Lummerzheim D., M. H. Rees, J. D. Craven and L. A. Frank, "Ionosheric conductances derived from DE-1 auroral images", *J. Atmos. Terr. Phys.*, **53**, 281–289, 1991.

Lyons L. R., T. L. Killeen and R. L. Walterscheid, "The neutral wind 'flywheelt' as a source of quiet-time, polar-cap currents", *Geophys. Res. Lett.*, **12**, 101–104, 1985.

Lysak R., "Propagation of Alfvén waves through the ionosphere", *Phys. Chem. Earth*, **22**, 757–766, 1997.

Lysak R., "Propagation of Alfvén waves through the ionosphere: Dependence on ionospheric parameters", *J. Geophys. Res.*, **104**, 10017–10030, 1999.

Lysak R., "Magnetosphere-ionosphere coupling by Alfvén waves at midlatitudes", *J. Geophys. Res.*, **109**, A07201, doi:10.1029/2004JA010454, 2004.

Lysak R. and Y. Song, "A three-dimensional model of the propagation of Alfvén waves through the auroral ionosphere: First results", *Adv. Space Res.*, **28**, 813–822, 2001.

Mayaud P. N., "Derivation, meaning and use of geomagnetic indices", ISBN 0-87590-022-4, *Geophysical monograph*, **22**, American Geophysical Union, 1980.

McPherron R., "Growth phase of magnetospheric substorms", *J. Geophys. Res.*, **75**, 5592–5599, 1970.

McPherron R. L., C. T. Russell and M. Aubry, "Satellite studies of magnetospheric substorms on August 15, 1978. 9. Phenomenological model for substorms", *J. Geophys. Res.*, **78**, 3131–3149, 1973.

Meng C.-I., M. Rycroft and L. Frank (editors), "Auroral Physics", ISBN 0-521-38049-9, *Cambridge University Press*, Cambridge, 1991.

Mersmann U., W. Baumjohann, F. Küppers and K. Lange, "Analysis of an eastward electrojet by means of upward continuation of ground-based magnetometer data", *J. Geophys.*, **45**, 281–298, 1979.

Murison M., A. Richmond, S. Matsushita and W. Baumjohann, "Estimation of ionospheric electric fields and currents from a regional magnetometer array", *J. Geophys. Res.*, **90**, 3525–3530, 1985.

Nygrén T., "Introduction to incoherent scatter measurements", ISBN 951-97489-0-3, *Invers Publications*, 1996.

Nygrén T., E. D. Tereshchenko, B. Z. Khudukon, O. V. Evstafiev, M. S. Lehtinen and M. Markkanen, "Manifestations of field-aligned currents in tomographic observations of the ionospheric F region", *Adv. Space Res.*, **26**, 939–942, 2000.

Ohtani S., R. Fujii, M. Hesse and R. Lysak (editors), "Magnetospheric current systems", ISBN 0-87590-976-0, *Geophysical monograph*, **118**, American Geophysical Union, 2000.

Olsen N., "Induction studies with satellite data", *Surveys in Geophysics*, **20**, 309–340, 1999.

Opgenoorth H. J., M. A. L. Persson, T. Pulkkinen and R. Pellinen, "Recovery phase of magnetospheric substorms and its association with morning sector aurora", *J. Geophys. Res.*, **99**, 4115–4129, 1994.

Palmroth M., "Solar wind - magnetosphere interaction as determined by observations and a global MHD simulation", PhD thesis, *Finnish Meteorological Institute Contributions*, **41**, 2003. Electronic version is available at [13].

Parks G., "Physics of space plasmas. An introduction", ISBN 0-201-48987-2, *Perseus books*, 1991.

Partamies N., P. Janhunen, K. Kauristie, T. Sergienko and S. Mäkinen, "Testing an inversion method for all-sky camera images", *Ann. Geophys.*, **22**, 1–11, 2004.

Paschmann G., S. Haaland and R. Treumann (editors), "Auroral Plasma Physics", *Space Sci. Rev.*, **103**, 1–486, 2002.

Pirjola R., "Electromagnetic induction in the Earth by a plane wave or by fields of line currents harmonic in time and space", *Geophysica*, **18**, 1–161, 1982.

Pirjola R., "Geomagnetic effects on ground-based technological systems", *Review of Radio Science 1999-2002*, edited by W. R. Stone, pp. 473–496, ISBN 0-471-26866-6, *John Wiley & Sons*, 2002.

Pirjola R. and A. Viljanen, "Complex image method for calculating electric and magnetic fields produced by an auroral electrojet of finite length", *Ann. Geophys.*, **16**, 1434-1444, 1998.

Polyakov S. V. and V. O. Rapoport, "Ionospheric Alfvén resonator", *Geomag. Aeronomy*, **21**, 610–614, 1981.

Popov V., V. Papitashvili and J. Watermann, "Modeling of equivalent ionospheric currents from meridian magnetometer chain data", *Earth Planets Space*, **53**, 129–137, 2001.

Pulkkinen A., O. Amm, A. Viljanen and BEAR Working Group, "Ionospheric equivalent current distributions determined with the method of spherical elementary current systems", *J. Geophys. Res.*, **108** (A2), 1053, doi:10.1029/2001JA005085, 2003a.

Pulkkinen A., O. Amm, A. Viljanen and BEAR Working Group, "Separation of the geomagnetic variation field on the ground into external and internal parts using the spherical elementary current system method", *Earth, Planets and Space*, **55**, 117–129, 2003b.

Pulkkinen A. and M. Engels "The role of 3-D geomagnetic induction in the determination of the ionospheric currents from the ground geomagnetic data", *Ann. Geophys.*, , **23**, 909–917, 2005.

Reigberg C., H. Lühr, P. Schwintzer and J. Wickert (editors), "Earth Observations with CHAMP. Results from Three Years in Orbit.", ISBN 3-540-22804-7, *Springer*, Berlin, 2005.

Rich F. and Y. Kamide, "Convection electric fields and ionospheric currents derived from model filed-aligned currents at high latitudes", *J. Geophys. Res.*, **88**, 271–281, 1983.

Richmond A. D., "Modeling the ionospheric wind dynamo: A review", *Pure and Applied Geophysics*, **131**, 413–435, 1989.

Richmond A. D. and Y. Kamide, "Mapping electrodynamic features of the high-latitude ionosphere from localized observations: Technique", *J. Geophys. Res.*, **93**, 5741–5759, 1988.

Richmond A. D., Y. Kamide, B.-H. Ahn at al., "Mapping electrodynamic features of the high-latitude ionosphere from localized observations: Combined incoherent-scatter radar and magnetometer measurements for January 18-19, 1984", *J. Geophys. Res.*, **93**, 5760–5776, 1988.

Richmond A. D. and J. P. Thayer, "Ionospheric Electrodynamics: A Tutorial", pp. 131–146 in Ohtani et al. (2000).

Rikitake T. and Y. Honkura, "Solid Earth Geomagnetism", ISBN 90-277-2120-3, *Terra Scientific Publishing Company*, Tokyo, 1985.

Robinson R. M., R. R. Vondrak, K. Miller, T. Dabbs and D. Hardy, "On calculating ionospheric conductances from the flux and energy of precipitating electrons", *J. Geophys. Res.*, **92**, 2565–2569, 1987.

Ruohoniemi J. and K. Baker, "Large-scale imagining of high-latitude convection with Super Dual Auroral Radar Network HF radar observations", *J. Geophys. Res.*, **103**, 20797–20811, 1998.

Scholer M., "On the motion of artificial ion clouds in the magnetosphere", *Planet. Space Sci.*, **18**, 977–1004, 1970.

Schunk R., and A. Nagy, "Ionospheres - Physics, plasma physics and chemistry", ISBN 0-521-63237-4, *Cambridge University Press*, Cambridge, 2000.

Sciffer M. D., C. Waters and F. W. Menk, "Propagation of ULF waves through the ionosphere: Inductive effect for oblique magnetic fields", *Ann. Geophys.*, **22**, 1155–1169, 2004.

Sharma A. S., Y. Kamide and G. S. Lakhina (editors), "Disturbances in Geospace: The Storm-Substorm Relationship", *Geophysical Monograph Series*, **142**, ISBN 0-87590-407-6, 2004.

Shirai H., Y. Kamide, E. A. Kihn et al., "Near Real-Time Calculation of Ionospheric Electric Fields and Currents Using GEDAS", *Chin. J. Astron. Astrophys.*, **3**, 375–380, 2003.

Stolle C., S. Schlüter, C. Jacobi, N. Jakowski, S. Heise and A. Raabe, "Three-dimensional Monitoring of the Polar Ionosphere with Ground- and Space-based GPS", pp. 477–482 in Reigberg at al. (2005).

Streltsov A. V. and W. Lotko, "Multiscale electrodynamics of the magnetosphere-ionosphere system", *J. Geophys. Res.*, **109**, A09214, doi:10.1029/2004JA010457, 2004.

Syrjäsuo M. and E. Donovan, "Diurnal auroral occurrence statistics obtained via machine vision", *Ann. Geophys.*, **22**, 1103–1113, 2004.

Tanskanen E., A. Viljanen, T. Pulkkinen, R. Pirjola, L. Häkkinen, A. Pulkkinen and O. Amm, "At substorm onset 40% of AL comes from underground", *J. Geophys. Res.*, **106** (A7), 13119–13134, 2001.

Thomson D. and J. Weaver, "The complex image approximation for induction in a multilayered Earth", *J. Geophys. Res.*, **80**, 123–129, 1975.

Toivanen P., H. Koskinen and T. Pulkkinen, "Mapping between the ionospheric and the tail electric fields in a time-dependent Earth's magnetosphere", *J. Geophys. Res.*, **103**, 9153–9164, 1998.

Untiedt J. and W. Baumjohann, "Studies of polar current systems using the IMS Scandinavian magnetometer array", *Space Sci. Rev.*, **63**, 245–390, 1993.

Viljanen A., A. Pulkkinen, O. Amm, R. Pirjola, T. Korja and BEAR Working Group, "Fast computation of the geoelectric field using the method of elementary current systems and planar Earth models", *Ann. Geophys.*, **22**, 101–113, 2004.

Vogt J., "Alfvén wave coupling in the auroral current circuit", *Surveys in Geophysics*, **23**, 335–377, 2002.

Vondrak R. and R. Robinson, “Inference of high-latitude ionization and conductivity from AE-C measurements of auroral electron fluxes”, *J. Geophys. Res.*, **90**, 7505–7512, 1985.

Wolf R. A. and Y. Kamide, “Inferring electric fields and currents from ground magnetometer data: A test with theoretically derived inputs”, *J. Geophys. Res.*, **88**, 8129–8135, 1983.

Yoshikawa A. and M. Itonaga, “Reflection of shear Alfvén waves at the ionosphere and the divergent Hall current”, *Geophys. Res. Lett.*, **23**, 101–104, 1996.

Yoshikawa A., M. Itonaga, S. Fujita, H. Nakata and K. Yumoto, “Eigenmode analysis of filed line oscillations interacting with the ionosphere-atmosphere-solid earth electromagnetic coupled system”, *J. Geophys. Res.*, **104**, 28437–28457, 1999.

Yoshikawa A. and M. Itonaga, “The nature of reflection and mode conversion of MHD-waves in the inductive ionosphere: Multistep mode conversion between divergent and rotational electric fields”, *J. Geophys. Res.*, **105**, 10565–10584, 2000.

Yoshikawa A., Y. Obana, M. Shinohara, M. Itonaga and K. Yumoto, “Hall-induced shielding effect on geomagnetic pulsations”, *Geophys. Res. Lett.*, **29**, doi:10.1029/2001GL013610, 2002.

Yoshikawa A., “Excitation of a Hall-current generator by field-aligned current closure, via an ionospheric, divergent Hall-current, during the transient phase of magnetosphere-ionosphere coupling”, *J. Geophys. Res.*, **107** (A12), 1445, doi:10.1029/2001JA009170, 2002.